Inorganic Chemistry

pubs.acs.org/IC Article

Mixed-Ligand Cobalt(III) Complexes of a Naturally Occurring Coumarin and Phenanthroline Bases as Mitochondria-Targeted Dual-Purpose Photochemotherapeutics

Tukki Sarkar, Arun Kumar,* Somarupa Sahoo, and Akhtar Hussain*

Cite This: *Inorg. Chem.* 2021, 60, 6649–6662 Read Online

ACCESS | Metrics & More | Article Recommendations | Supporting Information

ABSTRACT: The bioessential nature of cobalt and the rich photochemistry of its coordination complexes can be exploited to develop potential next-generation photochemotherapeutics. A series of six novel mixed-ligand cobalt(III) complexes of the formulation $[Co(B)_2(L)]ClO_4$ (**1**–**6**), where B is an N,N-donor phenanthroline base, namely, 1,10-phenanthroline (phen in **1** and **4**), dipyrido[3,2-*d*:2′,3′-*f*]quinoxaline (dpq in **2** and **5**), and dipyrido[3,2-*a*:2′,3′-*c*]phenazine (dppz in **3** and **6**), and L is an O,O-donor dianionic ligand derived from catechol (1,2-dihydroxybenzene, cat^{2-}, in **1**–**3**) or esculetin (6,7-dihydoxycoumarin, esc^{2-}, in **4**–**6**), have been prepared and characterized, and their light-triggered cytotoxicity has been studied in cancer cells. The single-crystal X-ray diffraction structures of complexes **1** (as PF_6^- salt, **1a**) and **2** show distorted octahedral geometries around the cobalt(III) center formed by the set of N_4O_2 donor atoms. The low-spin and 1:1 electrolytic complexes **1**–**6** display a d–d transition around 700 nm. Complexes **4**–**6** with a coordinated esc^{2-} ligand additionally display a $\pi \rightarrow \pi^*$ intraligand transition centered at 403 nm. Complexes **4**–**6** possessing a naturally occurring and photoactive esc^{2-} ligand show high visible-light-triggered cytotoxicity against HeLa and MCF-7 cancer cells, yielding remarkably low micromolar IC_{50} values while being much less toxic under dark conditions. Control complexes **1**–**3** possessing the photoinactive cat^{2-} ligand show significantly less cytotoxicity either in the presence of light or in the dark. The complex-induced cell death is apoptotic in nature caused by the formation of reactive oxygen species via a type 1 photoredox pathway. Fluorescence microscopy of HeLa cells treated with complex **6** reveals mitochondrial localization of the complex. A significant decrease in the dark toxicity of free esculetin and dppz base is observed upon coordination to cobalt(III). Complexes bind to calf-thymus DNA with significant affinity, but **6** binds with the greatest affinity. Complex **6** efficiently photocleaves supercoiled DNA to its nicked circular form when irradiated with visible light via a photoredox type 1 pathway involving hydroxyl radicals ($HO^{\bullet}$). Thus, complex **6** showing remarkable visible-light-triggered cytotoxicity but negligible toxicity in the dark is a good candidate for cancer photochemotherapy applications.

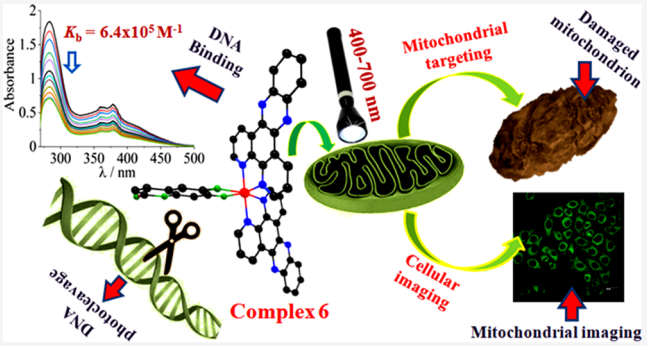

1. INTRODUCTION

Transition-metal complexes that can trigger cancer cell death upon irradiation by low-energy visible light have emerged as next-generation photochemotherapeutics in the treatment of cancer.[1−4] Photodynamic therapy (PDT) is a relatively recent example of photochemotherapy in which a photosensitizer (typically an organic molecule or a metal complex) generates cell-damaging reactive oxygen species (ROS) in the presence of light and molecular oxygen, leading to cancer cell death.[5] PDT has several advantages over the conventionally used therapies such as its spatiotemporal control, selectivity, negligible invasiveness, repeatability, and ability to circumvent drug resistance.[2,5] The currently used hematoporphyrin-based clinical PDT drug Photofrin suffers from several drawbacks such as long half-life (leading to prolonged skin photosensitivity), acute hepatotoxicity, and poor chemical purity. Therefore, considerable research efforts have been expended in the recent years to develop alternative photosensitizer drugs for cancer PDT.[6] Transition-metal complexes with their versatile structural aspects, useful redox chemistry, photophysical properties, and novel mechanism of action have shown promise as next-generation nonporphyrinic photosensitizers.[7,8] An example is the ruthenium complex TLD1433, which is currently in clinical trials for the PDT of bladder cancer.[8] Similarly, luminescent metal complexes showing emission in the visible region are of importance because of their usefulness as cellular imaging agents.[3,9,10] The emission

Received: February 12, 2021
Published: April 15, 2021

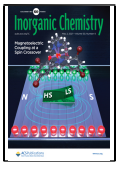

https://doi.org/10.1021/acs.inorgchem.1c00444
Inorg. Chem. 2021, 60, 6649–6662

property of a complex can be exploited to study its localization in specific subcellular organelles by confocal microscopy. Thus, a metal complex photosensitizer with emission property can be utilized as a dual-purpose phototheranostic agent.[9,10]

Among the transition-metal-based photosensitizers, complexes of bioessential transition-metal ions have received a great deal of current attention.[3,11−15] The bioessential nature of such metal ions would significantly lower the undesirable metal-induced intrinsic toxicity of a complex, which is a major problem with the platinum-based clinical chemotherapy drugs.[11−16] In this direction, oxovanadium(IV), iron(III), copper(II), and zinc(II) complexes have been extensively studied as photocytotoxic agents.[11−16] In contrast, complexes of bioessential cobalt(III) metal ion have been little explored as potential photochemotherapeutics.[17,18] Literature reports have shown that cobalt(III) complexes can be suitably designed as potential anticancer agents.[19] An interesting class of cobalt(III) complexes have been studied as hypoxia-activated pro-drugs.[20] Cobalt(III) complexes with their rich photochemical/photophysical properties and low-energy visible absorption band can be suitably designed as potential photocytotoxic drugs. Very recently, mixed-ligand cobalt(III) complexes of curcumin were shown to release the coordinated curcumin ligand upon visible-light irradiation.[21] We have recently reported mixed-ligand cobalt(III) complexes of curcumin that show visible-light-promoted cytotoxicity against cancer cells.[22]

Natural products have gained popularity as emerging sources for developing anticancer drugs, and the role of natural products in designing PDT drugs has recently been highlighted.[23,24] Esculetin (6,7-dihydroxycoumarin) is a naturally occurring coumarin derivative found in plants and is known to possess significant anticancer activity against various cancers.[25] Studies have shown that esculetin can act as a photosensitizer for DNA damage.[26] Although the photosensitizing properties of coumarins are reported, studies that focus on the photodynamic action of coumarins in a metal-bound form are scarce.[26] Very recently, we have reported a ferrocene-conjugated iron(III) complex of esculetin that shows significant light-induced cytotoxicity against cancer cells.[27] However, cobalt(III) coumarin complexes as photocytotoxic agents have not been explored.

There is currently a great interest in developing metal complexes that target mitochondria and inhibit their functions for applications in cancer therapy, mainly because of their manifold advantages over the nucleus-targeting anticancer drugs.[28] The problem of drug resistance in cisplatin chemotherapy stems from the repair of cisplatin−DNA adducts by the nucleotide excision repair mechanism of cells whereby the normal functions of DNA are restored.[29] Because mitochondria do not possess such a repair mechanism, they suffer from irreversible drug-induced damage, thereby offering an effective therapeutic strategy to address the problem of drug resistance in cancer chemotherapy.

The present work arises from our interest to develop novel mixed-ligand cobalt(III) complexes as dual-purpose photochemotherapeutics by exploiting the photosensitizing and emission properties of a naturally occurring coumarin (esculetin) and phenanthroline bases. In this paper, we report the synthesis, characterization, light-triggered cytotoxicity, cellular imaging, DNA binding affinity, and DNA photocleavage activity of six mixed-ligand cobalt(III) complexes of the formulation $[Co(B)_2(L)]ClO_4$ (**1**−**6**), where B is an N,N-donor phenanthroline base, namely, 1,10-phenanthroline (phen in **1** and **4**), dipyrido[3,2-*d*:2′,3′-*f*]quinoxaline (dpq in **2** and **5**), and dipyrido[3,2-*a*:2′,3′-*c*]phenazine (dppz in **3** and **6**), and L is an O,O-donor dianionic ligand derived from catechol (1,2-dihydroxybenzene, cat^{2-}, in **1**−**3**) or esculetin (6,7-dihydoxycoumarin, esc^{2-}, in **4**−**6**). The strongly coordinating phenanthroline bases, namely, phen, dpq, and dppz, are known to form thermodynamically stable complexes with cobalt(III).[17,18,30] Furthermore, the dppz ligand with its extended planar aromatic structure is well-known to act as a chelating photosensitizer ligand for transition-metal ions.[17,18,30] The cobalt(III) complexes (**1**−**3**) with the catecholate (cat^{2-}) ligand have been synthesized as controls to study the role of the photoactive esculetin ligand (esc^{2-}) in the overall activity of the complexes (Chart 1). Notable

Chart 1. Schematic Representation of Complexes 1−6

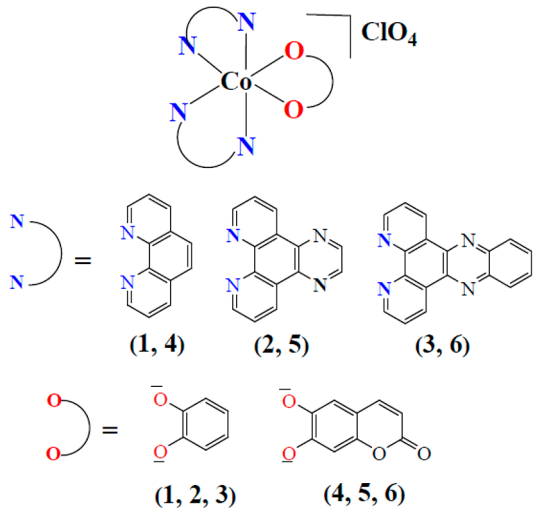

findings of this study include the (a) potent visible-light-induced cytotoxicity but negligible dark toxicity of complex **6** against cancer cells, (b) mitochondrial accumulation of complex **6**, (c) significant decrease in the dark toxicity of the esculetin and dppz ligands upon coordination to cobalt(III), (d) significant DNA binding affinity of the complexes, (e) efficient visible-light-induced DNA cleavage activity of complex **6** via a type I photoredox pathway, and (f) ability of complex **6** to serve as a cellular imaging agent.

2. EXPERIMENTAL SECTION

Materials and Methods. Reagents and chemicals used in this work were obtained from commercial suppliers (Sigma-Aldrich, U.S.A.; Alfa Aesar, U.K.; HiMEDIA, India) and used as received. Solvents were purified before use by standard purification techniques.[31] Esculetin, ethidium bromide (EB), calf-thymus (ct-) DNA (cesium chloride purified), and supercoiled DNA (SC-pUC19-DNA) were purchased from Sigma (U.S.A.). Tris(hydroxymethyl)-aminomethane-HCl (Tris-HCl; pH = 7.2) and phosphate-buffered saline (PBS; pH = 7.2) solutions was prepared using deionized and double distilled water (H_2O). Dulbecco's modified Eagle's medium (DMEM), Hoechst 33342, propidium iodide, 3-(4,5-dimethylthiazol-2-yl)-2,5-diphenyltetrazolium bromide (MTT), 9,10-anthracenediylbis(methylene)dimalonic acid (ABDA), 2′,7′-dichlorofluorescein diacetate (DCFDA), superoxide dismutase (SOD), and catalase were procured from Sigma-Aldrich (U.S.A) and used as received. Mito-Tracker Red (MTR) was procured from Invitrogen, U.S.A. The precursor 1,10-phenanthroline-5,6-dione was prepared as

https://doi.org/10.1021/acs.inorgchem.1c00444
Inorg. Chem. 2021, 60, 6649−6662

reported earlier.[32] The heterocyclic bases, namely, dipyrido[3,2-*d*:2′,3′-*f*]quinoxaline (dpq) and dipyrido[3,2-*a*:2′,3′-*c*]phenazine (dppz), were synthesized from 1,10-phenanthroline-5,6-dione by following previous reports.[33] Anhydrous $CoCl_2$ was synthesized by heating $CoCl_2{\cdot}6H_2O$. The complete removal of H_2O in the anhydrous sample was confirmed by Fourier transform infrared (FT-IR) spectroscopy, showing the complete absence of the broad −OH stretching of H_2O. The precursor cobalt(III) complexes $[Co(B)_2Cl_2]Cl$ (B = phen, dpq, and dppz) were prepared by oxidizing the corresponding cobalt(II) complexes using dry chlorine gas.[34] Dry chlorine gas was prepared in situ by reacting $KMnO_4$ with concentrated hydrochloric acid and passing the resulting gas through concentrated sulfuric acid.[23]

Caution! *Chlorine gas, being harmful and oxidizing, was handled cautiously inside a fume hood.*

The elemental (CHN) analyses of complexes **1**−**6** were performed using a Thermo Finnigan Flash EA 1112 analyzer. The IR spectra were obtained on a Bruker ATR FT-IR spectrometer. The electronic absorption spectra were recorded on an Elico SL 210 UV−visible spectrophotometer. Molar conductivities were recorded on a digital conductivity meter (Labtronics, India). The ^1H and ^{13}C NMR spectra were recorded at room temperature on a Bruker 400 MHz NMR spectrometer. Cyclic and square-wave voltammetry measurements were conducted on a Biologic SP-50 potentiostat/galvanostat (Biologic Instruments, France) equipped with a three-electrode setup comprised of a glassy carbon working electrode, a platinum wire auxiliary electrode, and a standard calomel reference electrode (SCE) at a scan speed of 100 mV s^{-1}. The square-wave voltammetry experiments were conducted at a pulse height (P_H) of 25 mV, a pulse width (P_W) of 50 ms, and a step height (S_H) of 10 mV. The experiments were carried out using a 10 mM solution of the complexes prepared in HPLC-grade dimethylformamide (DMF). Tetrabutylammonium perchlorate (TBAP; 0.1 M) was used as the supporting electrolyte. Electrospray ionization mass spectrometry (ESI-MS) spectra were recorded using Agilent Technologies 6538 UHD Accurate-mass Q-TOF LC/MS and Bruker Daltonics (Esquire 300 Plus ESI) mass spectrometers. The fluorescence spectra and fluorescence emission quantum yield (Φ) were measured using a Shimadzu (Japan) RF-6000 fluorescence spectrometer (reference: coumarin-153 dye, Φ = 0.56 in acetonitrile).[35] The emission intensity was calculated using *Origin 2020b* software, and the values of Φ were calculated by using the equation $\Phi_S/\Phi_R = (a_S/a_R)(A_R/A_S)(n_S^2/n_R^2)$, where Φ_S and Φ_R are the quantum yields of the sample and reference, respectively, a_S and a_R are the areas under the fluorescence spectra of the sample and reference, respectively, A_S and A_R are the respective absorbances of the sample and reference solution at the wavelength of excitation, and n_S and n_R are the respective refractive indices of the solvents used.[36] The confocal microscopic investigations were carried out using an Olympus FV 3000 confocal microscope. Flow cytometry analysis was performed using a FACS Calibur (Becton Dickinson) cell analyzer at the FL1 channel (595 nm).

Synthesis of Complexes 1−6. The complexes were synthesized by a general synthetic route in which a methanol suspension (10 mL) of the precursor complex $[Co(B)_2Cl_2]Cl$ (0.524 g of phen, 0.628 g of dpq, and 0.728 g of dppz; 1.0 mmol) was reacted with a methanol solution (10 mL) of H_2L (H_2cat, 0.101 g; H_2esc, 0.368 g; 1.0 mmol). Triethylamine (0.20 g, 2.0 mmol) taken in 5 mL of methanol was then added in a dropwise manner with constant stirring to the above reaction mixture. The mixture was stirred at room temperature for 2 h, during which the suspension slowly turned into a reddish-brown solution. The reaction mixture was filtered to remove any insoluble impurities. Isolation of the reddish-brown precipitate of the desired complex from the solution was accomplished by adding a methanol solution (5 mL) of $NaClO_4{\cdot}H_2O$ (0.14 g, 1.0 mmol) and allowing it to stand for 1 h at room temperature. The precipitate was filtered and washed with ice-cold methanol (10 mL), followed by diethyl ether. For complex **1a**, NH_4PF_6 (0.164 g, 1.0 mmol) was used instead of $NaClO_4{\cdot}H_2O$. For complexes **3** and **6**, the precipitate was redissolved in a mixture of dichloromethane/methanol [1:1 (v/v), 20 mL], and the resulting solution was filtered. Slow evaporation of the solution at room temperature afforded a brown microcrystalline solid, which was collected, washed with diethyl ether, and finally dried in a vacuum over phosphorus pentoxide.

Caution! *Metal perchlorates are potentially explosive in nature and should be handled with care.*

[Co(phen)$_2$(cat)]ClO$_4$ ***(1)***. Yield: ∼82%. Anal. Calcd for $C_{30}H_{20}N_4O_6ClCo$: C, 57.48; H, 3.22; N, 8.94. Found: C, 57.61; H, 3.27; N, 8.88. ESI-MS in aqueous acetonitrile [1:20 (v/v)]. Calcd for $[M - (ClO_4^-)]^+$: *m*/*z* 527.0978. Found: *m*/*z* 527.1028. FT-IR (cm^{-1}): 1577 w, 1523 m, 1475 s, 1425 m, 1345 w, 1318 w, 1252 vs, 1204 w, 1145 w, 1080 vs, 840 s, 789 m, 747 m, 717 s, 672 w, 655 m, 621 s (vs, very strong; s, strong; m, medium; w, weak). UV−visible [1:9 (v/v) DMF/PBS; λ_{max}, nm (ε, M^{-1} cm^{-1})]: 273 (54000), 300 sh (26000), 357 sh (3100), 762 (206). Molar conductivity in DMF at 298 K [Λ_M, S cm^2 mol^{-1}]: 85. ^1H NMR (DMSO-d_6): δ 9.14 (d, 2H, 2phen), 9.07 (d, 2H, 2phen), 8.90 (d, 2H, 2phen), 8.50 (d, 2H, 2phen), 8.41 (d, 2H, 2phen), 8.37−8.33 (m, 2H, 2phen), 7.83 (d, 2H, 2phen), 7.79−7.74 (m, 2H, 2phen), 6.45 (d, 2H, cat^{2-}), 6.18 (d, 2H, cat^{2-}) (s, singlet; d, doublet; m, multiplet). ^{13}C NMR (DMSO-d_6): δ 160.10 (2C, cat^{2-}), 153.19 (4C, 2phen), 151.67 (4C, 2phen), 146.97 (4C, 2phen), 140.36 (4C, 2phen), 130.90 (4C, 2phen), 127.52 (4C, 2phen), 116.86 (2C, cat^{2-}), 115.28 (cat^{2-}).

[Co(dpq)$_2$(cat)]ClO$_4$ ***(2)***. Yield: ∼78%. Anal. Calcd for $C_{34}H_{20}N_8O_6ClCo$: C, 55.87; H, 2.76; N, 15.33. Found: C, 55.96; H, 2.81; N, 15.37. ESI-MS in aqueous acetonitrile [1:20 (v/v)]. Calcd for $[M - (ClO_4^-)]^+$: *m*/*z* 631.1041. Found: *m*/*z* 631.1021. FT-IR (cm^{-1}): 1578 w, 1473 s, 1406 m, 1388 m, 1249 s, 1205 w, 1083 vs, 811 m, 723 s, 672 w, 625 s. UV−visible [1:9 (v/v) DMF/PBS; λ_{max}, nm (ε, M^{-1} cm^{-1})]: 270 (48100), 295 sh (38000), 346 sh (6700), 744 (238). Molar conductivity in DMF at 298 K [Λ_M, S cm^2 mol^{-1}]: 78. ^1H NMR (DMSO-d_6): δ 9.85 (d, 2H, 2dpq), 9.62 (d, 2H, 2dpq), 9.36 (s, 4H, 2dpq), 9.25 (d, 2H, 2dpq), 8.51−8.46 (m, 2H, 2dpq), 8.04 (d, 2H, 2dpq), 7.95−7.90 (m, 2H, 2dpq), 6.56 (d, 2H, cat^{2-}), 6.22 (d, 2H, cat^{2-}). ^{13}C NMR (DMSO-d_6): δ 159.77 (2C, cat^{2-}), 154.81 (4C, 2dpq), 152.62 (4C, 2dpq), 149.11 (4C, 2dpq), 147.26 (4C, 2dpq), 139.72 (4C, 2dpq), 136.94 (4C, 2dpq), 127.87 (4C, 2dpq), 117.48 (2C, cat^{2-}), 115.63 (2C, cat^{2-}).

[Co(dppz)$_2$(cat)]ClO$_4$ ***(3)***. Yield: ∼73%. Anal. Calcd for $C_{42}H_{24}N_8O_6ClCo$: C, 60.70; H, 2.91; N, 13.48. Found: C, 60.85; H, 2.85; N, 13.43. ESI-MS in aqueous acetonitrile [1:20 (v/v)]. Calcd for $[M - (ClO_4^-)]^+$: *m*/*z* 731.1354. Found: *m*/*z* 731.1393. FT-IR (cm^{-1}): 1577 w, 1499 w, 1475 s, 1421 m, 1349 m, 1340 w, 1246 s, 1072 vs, 813 w, 770 m, 717 s, 621 s, 570 m. UV−visible [1:9 (v/v) DMF/PBS; λ_{max}, nm (ε, M^{-1} cm^{-1})]: 275 (86300), 361 (21500), 377 (20000), 714 (227). Molar conductivity in DMF at 298 K [Λ_M, S cm^2 mol^{-1}]: 70. ^1H NMR (DMSO-d_6): δ 9.98 (d, 2H, 2dppz), 9.75 (d, 2H, 2dppz), 9.35−9.28 (m, 2H, 2dppz), 8.62−8.57 (m, 8H, 2dppz), 8.26−8.04 (m, 6H, 2dppz), 6.71 (d, 2H, cat^{2-}), 6.31 (d, 2H, cat^{2-}). ^{13}C NMR (DMSO-d_6): δ 159.78 (2C, cat^{2-}), 145.67 (4C, 2dppz), 142.23 (4C, 2dppz), 140.38 (4C, 2dppz), 140.12 (4C, 2dppz), 138.46 (4C, 2dppz), 130.06 (4C, 2dppz), 128.80 (4C, 2dppz), 127.21 (4C, 2ddpz), 124.70 (4C, 2dppz), 120.33 (2C, cat^{2-}), 109.62 (2C, cat^{2-}).

[Co(phen)$_2$(esc)]ClO$_4$ ***(4)***. Yield: ∼84%. Anal. Calcd for $C_{33}H_{20}N_4O_8ClCo$: C, 57.04; H, 2.90; N, 8.06. Found: C, 57.21; H, 2.84; N, 8.11. ESI-MS in aqueous acetonitrile [1:20 (v/v)]. Calcd for $[M - (ClO_4^-)]^+$: *m*/*z* 595.0816. Found: *m*/*z* 595.0836. FT-IR (cm^{-1}): 1704 s, 1580 m, 1520 w, 1481 s, 1433 m, 1378 m, 1270 s, 1250 m, 1186 w, 1081 vs, 915 m, 872 w, 835 s, 807 m, 746 w, 720 s, 650 w, 615 s. UV−visible [1:9 (v/v) DMF/PBS; λ_{max}, nm (ε, M^{-1} cm^{-1})]: 275 (56100), 402 (17200), 705 (247). Molar conductivity in DMF at 298 K [Λ_M, S cm^2 mol^{-1}]: 84. ^1H NMR (DMSO-d_6): δ 9.21 (d, 2H, 2phen), 9.17 (d, 2H, 2phen), 9.12 (d, 2H, 2phen), 9.05 (d, 2H, 2phen), 8.92 (d, 2H, 2phen), 8.52−8.35 (m, 2H, 2phen), 7.88 (d, 2H, 2phen), 7.83−7.76 (m, 2H, 2phen), 7.59 (d, 1H, esc^{2-}), 6.63 (s, 1H, esc^{2-}), 6.48 (s, 1H, esc^{2-}), 5.85 (d, 1H, esc^{2-}). ^{13}C NMR (DMSO-d_6): δ 167.11 (1C, esc^{2-}), 161.56 (1C, esc^{2-}), 158.45 (1C, esc^{2-}), 154.08 (1C, esc^{2-}), 149.58 (4C, 2phen), 144.61 (4C, 2phen), 141.04 (4C, 2phen), 140.25 (4C, 2phen), 130.32 (4C, 2phen), 128.47 (4C, 2phen), 127.21 (1C, esc^{2-}), 110.67 (1C, esc^{2-}), 109.87 (1C, esc^{2-}), 107.95 (1C, esc^{2-}), 103.00 (1C, esc^{2-}).

https://doi.org/10.1021/acs.inorgchem.1c00444
Inorg. Chem. 2021, 60, 6649−6662

[Co(dpq)$_2$(esc)]ClO$_4$ (**5**). Yield: ∼80%. Anal. Calcd for $C_{37}H_{20}N_8O_8ClCo$: C, 55.62; H, 2.52; N, 14.02. Found: C, 55.77; H, 2.56; N, 13.94. ESI-MS in aqueous acetonitrile [1:20 (v/v)]. Calcd for $[M - (ClO_4^-)]^+$: *m*/*z* 699.0939. Found: *m*/*z* 699.1175. FT-IR (cm^{-1}): 1692 m, 1580 w, 1529 s, 1400 m, 1385 s, 1289 vs, 1252 m, 1192 w, 1084 vs, 927 w, 813 m, 723 m, 621 m, 518 w. UV−visible [1:9 (v/v) DMF/PBS; λ_{max}, nm (ε, M^{-1} cm^{-1})]: 273 (61100), 345 (11500), 403 (16300), 691 (253). Molar conductivity in DMF at 298 K [Λ_M, S cm^2 mol^{-1}]: 73. ^{1}H NMR (DMSO-d_6): δ 9.83 (d, 2H, 2dpq), 9.61 (d, 2H, 2dpq), 9.35 (d, 2H, 2dpq), 9.30−9.21 (m, 2H, 2dpq), 8.52 (s, 4H, 2dpq), 8.06 (d, 2H, 2dpq), 7.99−7.93 (m, 2H, 2dpq), 7.64 (d, 1H, esc^{2-}), 6.73 (s, 1H, esc^{2-}), 6.57 (s, 1H, esc^{2-}), 5.81 (d, 1H, esc^{2-}). ^{13}C NMR (DMSO-d_6): δ 161.67 (1C, esc^{2-}), 154.92 (1C, esc^{2-}), 149.48 (1C, esc^{2-}), 147.15 (1C, esc^{2-}), 144.49 (4C, 2dpq), 142.56 (4C, 2dpq), 141.82 (1C, esc^{2-}), 139.55 (4C, 2dpq), 138.82 (4C, 2dpq), 137.06 (4C, 2dpq), 130.31 (4C, 2dpq), 128.21 (4C, 2dpq), 115.62 (1C, esc^{2-}), 112.95 (1C, esc^{2-}), 108.37 (1C, esc^{2-}), 98.03 (1C, esc^{2-}).

[Co(dppz)$_2$(esc)]ClO$_4$ (**6**). Yield: ∼70%. Anal. Calcd for $C_{45}H_{24}N_8O_8ClCo$: C, 60.11; H, 2.69; N, 12.46. Found: C, 60.21; H, 2.72; N, 12.42. ESI-MS in aqueous acetonitrile [1:20 (v/v)]. Calcd for $[M - (ClO_4^-)]^+$: *m*/*z* 799.1252. Found: *m*/*z* 799.1277. FT-IR (cm^{-1}): 1677 s, 1580 m, 1535 m, 1480 vs, 1252 s, 1180 m, 1138 w, 1078 s, 1048 w, 930 w, 813 m, 771 m, 730 m, 621 m, 573 w. UV−visible [1:9 (v/v) DMF/PBS; λ_{max}, nm (ε, M^{-1} cm^{-1})]: 283 (83500), 360 (26500), 377 (28100), 403 sh (15500), 685 (256). Molar conductivity in DMF at 298 K [Λ_M, S cm^2 mol^{-1}]: 71. ^{1}H NMR (DMSO-d_6): δ 9.98 (d, 2H, 2dppz), 9.76 (d, 2H, 2dppz), 9.34−9.24 (m, 2H, 2dppz), 8.58−8.40 (m, 8H, 2dppz), 8.25−7.80 (m, 2H, 2dppz), 7.68 (d, 1H of esc^{2-}), 7.05 (d, 2H, 2dppz), 6.80 (s, 1H, esc^{2-}), 6.67 (s, 1H, esc^{2-}), 6.20 (d, 2H, 2dppz), 5.80 (d, 1H, esc^{2-}). ^{13}C NMR (DMSO-d_6): δ 161.75 (1C, esc^{2-}), 152.42 (1C, esc^{2-}), 151.23 (1C, esc^{2-}), 147.92 (1C, esc^{2-}), 144.81 (4C, 2dppz), 142.69 (4C, 2dppz), 141.70 (1C, esc^{2-}), 140.84 (4C, 2dppz), 139.19 (4C, 2dppz), 137.53 (4C, 2dppz), 129.90 (4C, 2dppz), 128.86 (4C, 2dppz), 125.95 (1C, esc^{2-}), 124.30 (4C, 2dppz), 111.73 (1C, esc^{2-}), 111.06 (1C, esc^{2-}), 106.56 (1C, esc^{2-}), 96.84 (1C, esc^{2-}).

X-ray Crystallography. The crystal structures of **1** as its PF_6^- salt (**1a**) and **2** were obtained by a single-crystal X-ray diffraction method. Single crystals were grown by slow evaporation of a solution of the complex in a DCM/acetone [1:2 (v/v)] mixture. Crystal mounting was done on a glass fiber with epoxy cement. All geometric and intensity data were collected at room temperature using an automated Bruker SMART APEX CCD diffractometer equipped with a fine-focus 1.75 kW sealed-tube Mo Kα X-ray source (λ = 0.71073 Å) with increasing ω (width of 0.3° per frame) at scan speeds of 6 s (**1a**) and 5 s (**2**) per frame. The intensity data were collected by a ω−2θ scan mode and corrected for Lorentz−polarization and absorption effects. The structures were solved by direct methods using *SHELX-2013* incorporated in *WinGX*.[37] Empirical absorption corrections were done using *SADABS*. The hydrogen atoms belonging to the complex were in their calculated positions and refined using a riding model. All non-hydrogen atoms were refined anisotropically.[38] The perspective views of the complexes were obtained by *ORTEP*.[39] Selected crystallographic data are given in Table S1. The chemically significant bond distances and bond angles are shown in Table 3. The deposition numbers assigned to **1a** and **2** are CCDC 2024548 and 2024774, respectively.

Computational Studies. Computational studies were performed using the B3LYP/LANL2DZ level of density functional theory (DFT).[40] The hybrid B3LYP functional and LANL2DZ basis set were used in all calculations, as incorporated in the *Gaussian 09* package. Visualizations of the DFT-optimized structures and the frontier molecular orbitals [highest occupied molecular orbital (HOMO) and lowest unoccupied molecular orbital (LUMO)] of the complexes were performed using *Chemcraft 1.7*. To ascertain stationary points, a further frequency test was performed.

Cell Culture. Human cervical carcinoma (HeLa) and human breast adenocarcinoma (MCF-7) cells were maintained in DMEM supplemented with 10% fetal bovine serum, 100 IU mL^{-1} penicillin, 100 μg mL^{-1} streptomycin, and 2 mM Glutamax at 37 °C in a humidified incubator at 5% CO_2. The adherent cultures were grown as monolayers and passaged once in 4−5 days (at around 80% confluence) by trypsinizing with 0.25% trypsin/ethylenediaminetetraacetic acid.

Cell-Based Measurements. The cytotoxicity of the complexes was studied using MTT assay in the presence of visible light (400−700 nm, 10 J cm^{-2}) and in the dark against HeLa and MCF-7 cells by following a reported procedure (see the Supporting Information).[41] The half-maximal inhibitory concentration (IC_{50}) was determined both in the presence of light and in the dark and expressed in micromolar units. The phototoxicity index (PI), expressed as the ratio of the IC_{50} value in the dark divided by the IC_{50} value under light irradiation [PI = IC_{50}(dark)/IC_{50}(light)], was then calculated. The complex-induced mechanism of cell death was investigated using fluorescein isothiocyanate (FITC)-labeled annexin-V (abbreviated as annexin-V-FITC) assay using HeLa cells (see the Supporting Information).[42] The cellular localization behavior of complex **6** (10 μM) was studied by fluorescence confocal microscopy using HeLa cells (see the Supporting Information).[13,22,28b]

ROS Generation. A total of 10 μL of a DCFDA stock solution (1.0 mM) was added to 2 mL of complex **2** (10 μM), and the 100 μL of PBS was added. The sample was irradiated with visible light (400−700 nm, 10 J cm^{-2}, Luzchem Photoreactor, Canada). The formation of ROS was monitored by recording the intensity of DCF (formed by the oxidation of DCFDA) at 525 nm.[43] ABDA was used as a probe for detecting the formation of any singlet oxygen ($^1O_2$) by complex **6** under visible-light irradiation. A stock solution (1 mM) of complex **6** was prepared in dimethyl sulfoxide (DMSO) and added to a ABDA (1.0 mM) stock solution in water to obtain a final concentration of 20 μM ABDA and 10 μM complex **6**. The decrease in absorbance of the anthracene-centered band of ABDA at 378 nm was monitored at an interval of 10 min of continuous irradiation with visible light (400−700 nm, 10 J cm^{-2}).[44] The peroxide colorimetric tests for the detection of hydrogen peroxide (H_2O_2) in the reaction medium were conducted by using the Quantofix peroxide test sticks as per the instructions provided by the manufacturer (Merck-Supelco). In a typical experiment, complex **6** (10 μM) in 1% DMSO/99% PBS (v/v) at room temperature was either kept in the dark or irradiated with visible light (400−700 nm, 10 J cm^{-2}, Luzchem Photoreactor, Canada). Formation of H_2O_2 was detected by immersing an otherwise colorless stick into the reaction medium and then noting any color change after 30 s. The development of color indicates a positive test for H_2O_2, whereas no color change indicates a negative test for H_2O_2.[45]

DNA Binding and Photocleavage Experiments. The interaction of complexes **1**−**6** with ct-DNA was studied by UV−visible spectroscopy, thermal denaturation, and viscosity measurements by following previously published methods (see the Supporting Information).[28b] The DNA photocleavage experiments were carried out using SC-pUC19-DNA by evaluating the ability of complexes **1**−**6** to cleave SC-DNA to its nicked-circular (NC) form by employing DNA agarose gel electrophoresis (see the Supporting Information).[39] The mechanistic studies of the DNA photocleavage activity of the complexes were performed by adding various $^1O_2$ quenchers (for the type 2 pathway) and radical scavengers (for the type 1 pathway) and subsequently observing the effect of these additives on the cleavage efficiency of the complexes (see the Supporting Information).[28b]

3. RESULTS AND DISCUSSION

Synthesis and General Aspects. The mixed-ligand cobalt(III) complexes $[Co(B)_2(L)]ClO_4$ (**1**−**6**) were synthesized in ∼75% yield by reacting the corresponding precursor cobalt(III) complexes $[Co(B)_2Cl_2]Cl$ with either H_2cat or H_2esc (after deprotonation by using triethylamine), followed by anion metathesis with $NaClO_4$ (Chart 1 and Figures S1 and S2). The satisfactory elemental (CHN) data confirmed the purity of the synthesized complexes. The FT-IR spectra of

https://doi.org/10.1021/acs.inorgchem.1c00444
Inorg. Chem. 2021, 60, 6649−6662

complexes **1**–**6** recorded on solid samples showed a strong stretching band at ~1080 cm^{-1}, which can be ascribed to the presence of the perchlorate (ClO_4^-) anion (Figures S3–S8).[46] In addition, complexes **4**–**6** possessing the esc^{2-} ligand showed a strong band at ~1690 cm^{-1} arising from the presence of the C═O moiety (Table 1 and Figures S6–S8).

Table 1. Selected Physicochemical Data for Complexes 1–6

complex	ESI-MS/ $(m/z)^a$	IR[b]/cm^{-1} (C═O)	log P^c	$K_b{}^d/M^{-1}$ [s]	$\Delta T_m{}^e$/ °C
1	527.1028		1.11	5.9 (±0.2) × 10^4 [0.1]	1.5
2	631.1021		1.25	3.4 (±0.3) × 10^5 [0.3]	3.3
3	731.1393		1.55	5.5 (±0.5) × 10^5 [0.4]	5.0
4	595.0836	1702	1.23	6.8 (±0.3) × 10^4 [0.2]	2.1
5	699.1175	1692	1.42	4.3 (±0.5) × 10^5 [0.3]	4.0
6	799.1277	1677	1.70	6.4 (±0.6) × 10^5 [0.4]	5.8

[a]Molecular-ion peak corresponding to $[M - (ClO_4^-)]^+$ species in aqueous acetonitrile. [b]Recorded on dry solid samples. [c]Octanol/water (o/w) partition coefficient. [d]K_b, DNA binding constant (*s*, binding site size). [e]Change in the DNA melting temperature.

The low-spin diamagnetic complexes showed 1:1 electrolytic behavior in DMF, as evidenced from the molar conductivity (Λ_M) data (Table 1).[47] The room temperature ^1H and ^{13}C NMR spectra of the complexes showed peaks corresponding to the coordinated phenanthroline bases and the cat^{2-}/esc^{2-} ligands, as evidenced from the shift in the peak positions due to coordination (Figures S9–S20). Interestingly, upon coordination to the cobalt(III) center, the sets of protons that were chemically equivalent in the free phenanthroline bases behaved differently and found to resonate at a slightly different δ value in the ^1H NMR spectra of the complexes. This observation is further supported by the fact that the Co–N bond distances are different for the two coordinated phenanthroline bases in the complexes, as evidenced from the X-ray structures of complexes **1** and **2**. The mass spectra (ESI-MS) of complexes **1**–**6** revealed essentially a single peak corresponding to the $[M - (ClO_4^-)]^+$ species in aqueous acetonitrile (Table 1 and Figures S21–S26). The observation of the $[M - (ClO_4^-)]^+$ peaks and the absence of any noticeable fragmentation peaks indicated that the complexes were stable in an aqueous solution. The UV–visible spectra of complexes **1**–**6** measured in DMF/PBS [1:9 (v/v), pH = 7.2] displayed a common absorption band at ~275 nm attributable to a $\pi \rightarrow \pi^*$ transition (Figures 1a and S27).[17,22] A common band at ~345 nm due to the n → π^* transition involving the quinoxaline moiety was observed for the dipyridoquinoxaline (dpq) complexes **2** and **5**.[17,22] For the dipyridophenazine (dppz) complexes **3** and **6**, two additional absorption bands at 361 and 377 nm were observed that can be attributed to the n → π^* transitions of the phenazine moiety.[17,22] Furthermore, complexes **4**–**6** showed an esculetin-based $\pi \rightarrow \pi^*$ visible absorption band at ~402 nm.[27] For the free esculetin molecule (H_2esc), the corresponding absorption occurs at ~347 nm. It follows that a bathochromic shift of this ligand-centered band is observed upon coordination to cobalt(III).[26b,27] The d^6 low-spin ($t_{2g}{}^6$) complexes also displayed a ligand-field d–d band in the range 650–800 nm originating from the $^1A_{1g} \rightarrow {}^1T_{2g}$ and

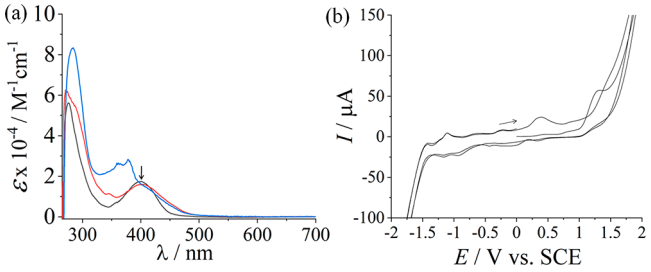

Figure 1. (a) Electronic absorption spectra of complexes **4** (black), **5** (red), and **6** (blue) in DMF/PBS [1:9 (v/v), pH = 7.2]. (b) Cyclic voltammograms (current vs potential plots) of complex **6** measured in 1:1 (v/v) DMF/PBS (vs SCE; 0.1 M TBAP) at a scan speed of 100 mV s^{-1} showing the cathodic and anodic peaks. The full cycle was observed by setting the number of repeat cycles (n_R) = 1.

$^1A_{1g} \rightarrow {}^1T_{1g}$ transitions (Figure S28).[48] For complexes **3** and **6**, while the longer-wavelength regions for the d–d transitions could be seen in the spectra, the shorter-wavelength regions were masked by the appearance of the high-intensity ligand-based transitions of the coordinated dppz bases. The short-wavelength intraligand transitions of the coordinated cat^{2-} and esc^{2-} ligands were also masked by the appearance of the high-intensity ligand-based transitions of the phenanthroline bases. The occurrence of absorption bands in the visible region allowed us to study the photochemotherapeutic anticancer activity of complexes **1**–**6**.[27] The catecholate complexes **1**–**3** were nonemissive because of the absence of any fluorophore moiety in their structures (Figure S29). In contrast, the esculetin complexes **4**–**6** showed an emission band centered at 503 nm (λ_{ex} = 402 nm) in DMF/PBS [1:9 (v/v)] due to the coordinated esc^{2-} ligand, giving quantum yield (Φ) values of ~0.01 (Figure S30).[26b,27] H_2esc emits at 465 nm (blue emission) when excited at 345 nm.[26b,27] Thus, the absorption and emission bands of esculetin shifted significantly upon binding to cobalt(III).[26b,27]

Cyclic and square-wave voltammetry studies of complexes **1**–**6** revealed a cobalt(III)/cobalt(II) response in the range −0.40 to −0.47 V versus SCE [−0.16 to −0.23 V vs normal hydrogen electrode (NHE)] in DMF/PBS (1:1)/0.1 M [^{n}Bu$_4$N]ClO_4 (Figures 1b and S31–S41).[17c] A catechol-based anodic response near +0.6 V versus SCE (+0.36 V vs NHE) was observed for complexes **1**–**3** without any cathodic counterpart. The corresponding response for the esculetin complexes **4**–**6** was observed near +0.80 V versus SCE (0.56 V vs NHE). Voltammetric responses for the coordinated phenanthroline bases were observed below −1.00 V versus SCE (−0.76 V vs NHE). For example, complexes **3** and **6** showed a dppz ligand-based voltammetric response near −1.04 V versus SCE (−0.81 V vs NHE). For the phen and dpq complexes, the corresponding response was observed near −1.10 V versus SCE (−0.86 V vs NHE). In addition, a common anodic response near +1.29 V versus SCE (+1.05 V vs NHE) originating from the coordinated phenanthroline bases was observed for all of the complexes. The free phenanthroline ligands, namely, phen, dpq, and dppz, exhibit a common cathodic response near −0.50 V versus SCE (+0.26 V vs NHE) and two common anodic responses near +0.43 and +1.28 V versus SCE (+0.19 and +1.04 V vs NHE; Figures S42–S44). Additionally, the free dppz ligand was found to display a quasi-reversible voltammetric response near −1.12 V versus SCE (−0.88 V vs NHE) with a i_{pa}/i_{pc} ratio of ~0.9.[49]

https://doi.org/10.1021/acs.inorgchem.1c00444
Inorg. Chem. 2021, 60, 6649–6662

The free esculetin ligand was found to exhibit one anodic response near +0.98 V versus SCE (+0.74 V vs NHE) and a cathodic response near +0.24 V versus SCE (0.00 V vs NHE; Figure S45). The voltammetric responses of the dppz complexes **3** and **6** were found to be poorer compared to that of the free dppz ligand. The redox data suggest the involvement of the cobalt(III) center and the coordinated ligands in the overall redox behavior of the complexes.[17]

Single-Crystal X-ray Diffraction Structures. The solid-state structures of complexes **1a** and **2** were obtained by a single-crystal X-ray diffraction method. **1a** crystallized in the space group $P\bar{1}$ of the triclinic crystal system with two molecules in the asymmetric unit, while **2** crystallized in the space group $P2_1/n$ of the monoclinic crystal system with four molecules in the asymmetric unit. The X-ray structures revealed that the complexes were mononuclear octahedral species with a coordination sphere formed by a CoN_4O_2 core involving the central cobalt(III) ion, two bidentate N,N-donor phenanthroline bases (phen for **1a** and dpq for **2**) and one bidentate O,O-donor cat^{2-} ligand. The ORTEP views of **1a** and **2** are shown in Figure 2, and the unit cell packing diagrams are given in Figures S46 and S47.

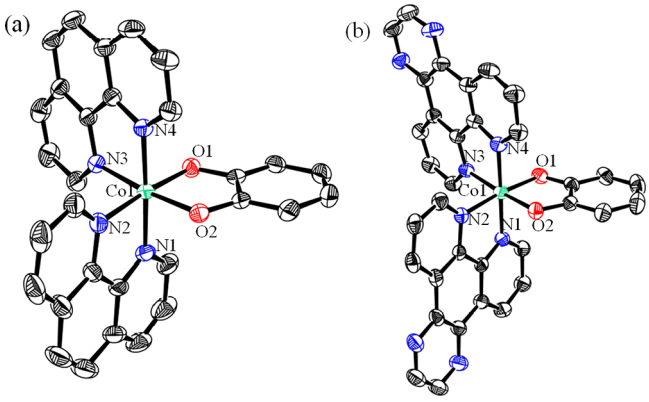

Figure 2. X-ray structures (ORTEP representation at 40% thermal ellipsoid probability) of (a) **1a** and (b) **2**. The hydrogen atoms and counteranion have been omitted for the sake of clarity.

The Co−N bond distances were within 1.935(3)−1.9674(17) Å, while the Co−O bond distances were within 1.8672(15)−1.882(3) Å. While all of the Co−O bond distances were nearly equal, the Co−N(1) and Co−N(4) bond distances [~1.937(3) Å] were slightly shorter than the Co−N(2) and Co−N(3) bond distances [~1.964(3) Å], suggesting a distorted octahedral geometry in both structures. The selected crystallography parameters are given in Table S1, and the bond lengths and angles are shown in Table 2.

Computational Studies. DFT calculations were carried out by using the B3LYP level theory with a LAN2DZ basis set with *Gaussian 09* programs to obtain the optimized geometries and insights into the excited-state properties of complexes **1**−**6**. The initial coordinates were obtained from the crystal structures and used for optimization. The frontier orbital calculations for the complexes showed that, for the phen (**1** and **4**) and dpq (**2** and **5**) complexes, the HOMOs are localized on either the cat^{2-} or esc^{2-} ligand and the LUMOs are spread over the two B ligands (Figures 3 and S48 and S49 and Tables S2−S7). For the dppz complexes **3** and **6**, the HOMOs are localized on the dppz ligand and the LUMOs are centered on the cat^{2-} or esc^{2-} ligand. The high phototoxicity

Table 2. Selected Bond Distances (Å) and Angles (deg) with the Estimated Standard Deviations (esd) in Parentheses

$[Co(phen)_2(cat)]PF_6$ (**1a**)			
Co1−O1	1.882(3)	N2−Co1−N3	94.75(13)
Co1−O2	1.876(3)	N2−Co1−N4	93.55(13)
Co1−N1	1.939(3)	N3−Co1−N4	83.92(13)
Co1−N2	1.962(3)	O1−Co1−N2	175.28(12)
Co1−N3	1.962(3)	O1−Co1−N3	88.07(12)
Co1−N4	1.935(3)	O1−Co1−N4	90.51(12)
N1−Co1−N2	84.20(15)	O1−Co1−O2	88.57(11)
N1−Co1−N3	94.98(13)	O2−Co1−N2	88.90(12)
N1−Co1−N4	177.41(12)	O2−Co1−N3	174.46(11)
N1−Co1−O1	91.79(13)	O2−Co1−N4	91.72(12)
N1−Co1−O2	89.52(13)		
$[Co(dpq)_2(cat)]ClO_4$ (**2**)			
Co1−O1	1.8716(15)	N2−Co1−N3	93.46(7)
Co1−O2	1.8672(15)	N2−Co1−N4	95.20(7)
Co1−N1	1.9362(17)	N3−Co1−N4	83.44(7)
Co1−N2	1.9674(17)	O1−Co1−N2	173.80(7)
Co1−N3	1.9617(18)	O1−Co1−N3	90.73(7)
Co1−N4	1.9389(18)	O1−Co1−N4	89.81(7)
N1−Co1−N2	83.45(7)	O1−Co1−O2	88.82(7)
N1−Co1−N3	96.43(7)	O2−Co1−N2	87.35(7)
N1−Co1−N4	178.64(7)	O2−Co1−N3	175.44(7)
N1−Co1−O1	91.55(7)	O2−Co1−N4	92.02(7)
N1−Co1−O2	92.02(7)		

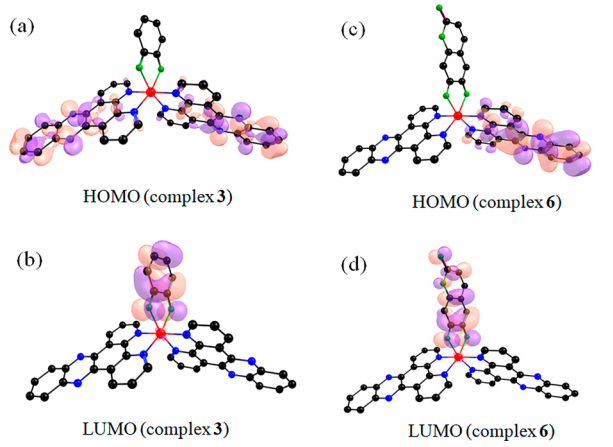

Figure 3. DFT-calculated HOMOs (part a for complex **3** and part c for complex **6**) and LUMOs (part b for complex **3** and part d for complex **6**). Color code: carbon, black; nitrogen, blue; oxygen, green. The hydrogen atoms are not shown.

observed for the dppz complexes **3** and **6** could be a result of a facile electronic transition originating from the coordinated photoactive dppz ligand to the available orbitals in the esc^{2-} ligand.[17,21,22]

Solubility, Stability, and Photostability. At room temperature, the complexes were soluble in acetone, acetonitrile, DMF, and DMSO. They were moderately soluble in water (~0.4−0.6 g L^{-1}; Table S8), methanol, ethanol, dichloromethane, and chloroform but insoluble in hydrocarbon solvents. To examine the biological activity of potential drug candidates, it is a prerequisite that they are stable in physiological conditions. Therefore, we studied the stability of the complexes by UV−visible spectroscopy. Complexes were stable in a 10% DMSO/DMEM medium (pH = 7.4, 37 °C), as evidenced from the absorption spectral study on complex **6**

https://doi.org/10.1021/acs.inorgchem.1c00444
Inorg. Chem. 2021, 60, 6649−6662

Table 3. IC_{50} Values of Complexes 1−6 and Other Relevant Compounds in HeLa and MCF-7 Cells

	HeLa			MCF-7		
compound	light[a]/μM	dark/μM	PI	light[a]/μM	dark/μM	PI
1	>50	>50		>50	>50	
2	28.9 ± 0.3	>50	>1.7	22.4 ± 0.2	>50	>2.2
3	5.0 ± 0.1	>50	>10.0	2.8 ± 0.1	>50	>17.8
4	20.1 ± 0.2	>50	>2.5	17.2 ± 0.2	>50	>6.9
5	10.0 ± 0.1	>50	>5.0	8.8 ± 0.1	>50	>5.6
6	1.6 ± 0.1	>50	>31.7	1.1 ± 0.1	>50	>45.9
esculetin[b]	18.2 ± 1.5	20.3 ± 1.4	1.1	11.4 ± 1.3	13.6 ± 1.2	1.2
dppz[c]	>100	11.6	<0.1			
[Co(L)dppz][d]	>100	>100				
[Co(mitocur)L]Cl_2[e]				3.9 ± 0.7	>50	>12.8
photofrin[f]	4.3 ± 0.2[f]	>41	>9.5			

[a]Light of 400−700 nm (10 J cm^{-2}) wavelength. [b]Reference 27. [c]Reference 49. [d]Reference 17b, [e]Reference 21b. [f]Reference 54 and light source reported: red light of 633 nm. PI = IC_{50}(dark)/IC_{50}(light).

showing no apparent spectral change even after 48 h (Figure S50). Furthermore, no significant spectral change was observed for complex **6** when irradiated by visible light at different time intervals (spectra were recorded every 20 min after irradiation for 5 min up to 4 h), suggesting that the complex was photostable and did not undergo photobleaching upon exposure to visible light. Next, we studied whether the cobalt(III) complexes can be reduced to cobalt(II) in the presence of reducing agents. In the presence of a slight excess of ascorbic acid (5 equiv) as the reducing agent, the fluorescence spectra of complex **6** in DMF/PBS (1:9) did not show any noticeable change. However, in the presence of a large excess of ascorbic acid (>100 equiv), a noticeable increase of the emission intensity of complex **6** was observed, suggesting that complex **6** did undergo a reduction from cobalt(III) to cobalt(II) (Figure S51).[17,21,22] In another experiment using reduced glutathione (GSH), similar results were obtained. A slight excess (5 equiv) of GSH did not have any significant effect on the emission intensity of complex **6**. In contrast, in the presence of an excess of GSH (>30 equiv), a significant increase of the emission intensity of complex **6** was observed, suggesting that a reduction from cobalt(III) to cobalt(II) took place (Figure S52). This observation is supported by the cyclic voltammetry results in that the potential for the cobalt(III)/cobalt(II) reduction for the complexes is in the range −0.16 to −0.21 V versus NHE, which is slightly more positive than the reduction potential for GSH (−0.24 V vs NHE). The reduction of complex **6** in the presence of GSH was further evidenced by the mass spectral measurements [aqueous acetonitrile, 1:20 (v/v)] of complex **6** treated with GSH (30 equiv) showing the presence of two additional peaks at *m*/*z* 332.11 and 320.60 (Figure S53). These two peaks correspond to the 5-coordinate species $[Co(dppz)_2(MeCN)]^{2+}$ and $[Co(dppz)_2(H_2O)]^{2+}$, respectively. The existence of such 5-coordinate species is well documented in the literature.[21a,50] The colorimetric test to detect the presence of cobalt(II) in the solution turned out to be negative, suggesting that only the catecholate/esculetin ligand is released from the complex, not the phenanthroline bases.[51]

Lipophilicity. The lipophilicity of a drug candidate is an important aspect that governs its cellular uptake by passive diffusion, localization in specific cellular organelles, metabolism, and excretion.[52] A more lipophilic drug is more likely to accumulate inside cells via diffusion through the hydrophobic lipid bilayer compared to a less lipophilic one. The lipophilicity of a drug can be evaluated by determining the o/w partition coefficient (*P*, expressed as log *P*). The shake-flask method was employed to determine log *P* of complexes **1**−**6** (see the Supporting Information). Complexes **1**−**3** having the cat^{2-} ligand gave log *P* values of 1.11 ± 0.04, 1.25 ± 0.06, and 1.55 ± 0.05, respectively, while complexes **4**−**6** having the esc^{2-} ligand gave log*P* values of 1.23 ± 0.03, 1.42 ± 0.04, and 1.70 ± 0.06, respectively (Table 1). Thus, the complexes with the cat^{2-} ligand were found to be less lipophilic compared to their respective esc^{2-} counterparts, which correlates well with the fact that H_2esc is more lipophilic (log *P* = 1.31) than the free catechol molecule (log *P* = 0.90).[27] The dppz complexes **3** and **6** were found to be more lipophilic than the dpq complexes **2** and **5**, which, in turn, were found to be more lipophilic than the phen complexes **1** and **4**. This order correlates well with the order of the lipophilicity of the phenanthroline bases dppz > dpq > phen.

Photocytotoxicity. The photochemotherapeutic anticancer activity of complexes **1**−**6** was studied by MTT assay (Table 3 and Figures S54−S65) in the presence of low-energy visible light (400−700 nm, 10 J cm^{-2}). The photocytotoxicities of the complexes were evaluated against two cancer cell lines, namely, HeLa and MCF-7. Complexes did not show any significant dark toxicity (IC_{50} > 50 μM) against the two tested cell lines, which is of importance considering the fact that an ideal PDT drug should not be toxic in the dark. Upon visible-light irradiation, complex **1**, lacking any photoactive moiety, did not exhibit any cytotoxic effect (IC_{50} > 50 μM) against both cell lines. Complex **2** having cat^{2-} and dpq as ligands exhibited a mild cytotoxic effect under similar conditions, giving an IC_{50} value of 28.89 μM (PI > 1.7) against HeLa cells and 22.41 μM (PI > 2.2) against MCF-7 cells. Notably, complex **3** having cat^{2-} and photoactive dppz as ligands showed significant cytotoxicity, yielding an IC_{50} value of 5.01 μM (PI > 10) against HeLa cell lines and 2.81 μM (PI > 17.8) against MCF-7 cell lines. Thus, among complexes **1**−**3**, the observed photocytotoxicity follows the order **3** > **2** > **1**. On the other hand, complex **4** having phen and photoactive esc^{2-} as ligands showed moderate cytotoxicity against both cell lines, with an IC_{50} value of 20.12 μM (PI > 2.5) against HeLa cell lines and 17.25 μM (PI > 6.9) against MCF-7 cell lines. For complex **5** with dpq and photoactive esc^{2-} ligands, the cytotoxicity was more pronounced (IC_{50} = 10.02 μM and PI > 5.0 against HeLa cells; IC_{50} = 8.84 μM and PI > 5.6 against

https://doi.org/10.1021/acs.inorgchem.1c00444
Inorg. Chem. 2021, 60, 6649−6662

MCF-7 cells) compared to that of complex **4**. Complex **6** having photoactive dppz and esc^{2-} ligands showed the most potent cytotoxic effect, yielding an IC_{50} value of 1.58 μM (PI > 31.7) against HeLa cells and 1.09 μM (PI > 45.9) against MCF-7 cells. Thus, among complexes **4**−**6**, the observed photocytotoxicity follows the order **6** > **5** > **4**. Thus, complexes **1**−**3** having photoinactive cat^{2-} ligands were less toxic compared to complexes **4**−**6** having photoactive esc^{2-} ligands (Table 3). The observed photocytotoxicity of the complexes correlates well with the observed lipophilicity, and the high lipophilicity of complex **6** could be a factor contributing to its potent phototoxicity against cancer cells. Similarly, among the phenanthroline bases, complexes **3** and **6** having the photoactive dppz ligand showed notably higher cytotoxicity compared to the dpq and phen complexes, which is attributable to the fact that the dppz ligand has its absorption tail extending into the visible region (Figure S27). This observation is corroborated by previous reports on similar oxovanadium(IV) and cobalt(III) complexes.[22,53] The phototoxicity of complex **6** is comparable to that of the clinical PDT drug Photofrin (IC_{50} = 4.2 μM against HeLa cells).[54] H_2esc is known to give the respective IC_{50} values of 18.2 and 11.4 μM in visible light and 20.3 and 13.6 μM in the dark against HeLa and MCF-7 cell lines.[27] Thus, the undesirable dark toxicity of the free esculetin ligand is decreased upon coordination to cobalt(III). The decrease in the dark toxicity of the esculetin ligand is of importance because a potential PDT drug should be nontoxic in the dark. Similarly, the free dppz ligand is also known to show significant dark toxicity (IC_{50} = 11.6 μM against HeLa cells),[49] which has been found to decrease upon coordination to cobalt(III). An ideal photochemotherapeutic drug should be highly toxic in the presence of light but negligibly toxic in the dark. Thus, the impressively high phototoxicity and negligible dark toxicity of complex **6**, combined with its high PI, render it a potential candidate amenable to in vivo study as a next-generation mitochondria-targeted photochemotherapeutic drug.

Cellular Localization. A cellular localization study can provide information on the accumulation of a drug in specific cellular organelles, which, in turn, can provide important information regarding the mechanism of its action.[3,11−15] In addition to displaying photocytotoxicity, if the photosensitizer drug shows emission in the visible region, its localization inside cells can be studied by imaging the cells using confocal microscopy. Thus, the photosensitizer can be used as a dual-purpose agent for therapy and cellular imaging. With this idea in mind, we exploited the green emission from complex **6** to study its localization in HeLa cells (Figure 4). Complex **6** accumulated primarily in the cytosol of HeLa cells, as evidenced from costaining with the nucleus staining dye Hoechst 33258 (blue emission, panel b). Furthermore, we studied the localization of complex **6** within the specific cytosolic organelles, particularly the mitochondria (panels g−i in Figure 4). Costaining of complex **6** (green emission) with the mitochondria staining dye MTR (deep-red emission, panel c) revealed that complex **6** localized primarily in the mitochondria, giving a Pearson correlation coefficient (a quantitative measure of the degree of colocalization) value of 0.85. The localization of complex **6** in the mitochondrion and its absence in the nucleus suggest that the mitochondrion is its primary target, not the nucleus. This finding is significant considering that mitochondrial damage induced by a drug triggers the intrinsic pathway of apoptosis.[17,22,28] Photocytotoxic cobalt(III) complexes with naturally occurring coumarin ligands showing mitochondrial localization are not documented in the literature.

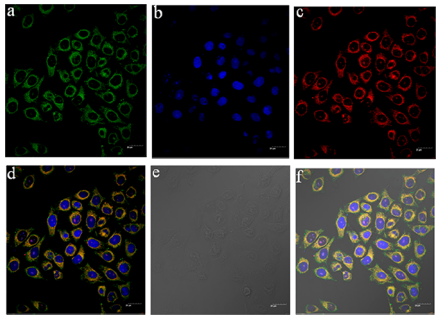

Figure 4. Confocal microscopy images of HeLa cells treated with complex **6** (10 μM) showing mitochondrial localization: (a) green emission from complex **6**; (b) blue emission from Hoechst 33258 (5 μg mL^{-1}) dye; (c) red emission from MTR (0.5 μM) dye; (d) merged images of complex **6** + Hoechst 33258 + MTR; (e) bright-field image; (f) merged images of panels d and e. Scale bar: 20 μm.

Annexin-V-FITC/PI Assay. It is important to delve into the mechanism of cell death induced by a photoactive drug. Apoptosis (a programmed cell death) is a well-known mechanism of cell death in cancer photochemotherapy.[1−5] The ability of complex **6** to trigger any apoptotic cell death was investigated by annexin-V-FITC/PI assay using HeLa cells (Figure 5). Annexin-V is a membrane protein having a strong calcium(II)-dependent affinity for phosphotidylserine (PS). In living cells, PS is transported to the inside of the lipid bilayer by aminophospholipid translocase, which is a magnesium(II) adenosine triphosphate-dependent enzyme. During apoptosis, PS is translocated from the cytoplasmic (inner) surface of the cell membrane to the outer surface. Annexin-V binds specifically to PS, and annexin-V-FITC can be used as a fluorescence probe to detect and quantify viable, apoptotic, and necrotic cell populations. The DNA binding dye propidium iodide (red fluorescence) can be used in conjunction with annexin-V-FITC (green fluorescence). Propidium iodide is excluded by viable and apoptotic cells but permeabilized only by necrotic cells. The results of this assay can be analyzed by fluorescence-assisted cell sorting, which gives an estimate of apoptotic cells at different stages of the cell death event: early apoptosis, high annexin-V-FITC [quadrant 4 (Q4)], low propidium iodide; late apoptosis, both high annexin-V-FITC and propidium iodide (Q2), viable cells [unstained, only showing autofluorescence (Q3)], and necrotic cell populations [stained with PI only (Q1)]. HeLa cells treated with complex **6** (4 μM) revealed no apparent apoptotic features in the dark (Figure 5b). In contrast, the characteristic features of early apoptosis induced by the complex were observed in ∼42% of the cell population upon irradiation with visible light (Figure 5c).

ROS Generation. Metal-based PDT photosensitizers are known to trigger cell death by generating ROS upon light irradiation, thereby rendering themselves photocytotoxic.[55] To know whether a type 2 ($^1O_2$) or type 1 (radical) pathway is involved, we used ABDA as a water-soluble probe for $^1O_2$ in the presence of complex **6** and visible light.[56] Treatment of complex **6** with ABDA, followed by irradiation with visible light, resulted in no noticeable decrease in the absorbance of the anthracene-centered band of ABDA at 378 nm, thereby ruling out the possibility of endoperoxide formation (Figure

https://doi.org/10.1021/acs.inorgchem.1c00444
Inorg. Chem. 2021, 60, 6649−6662

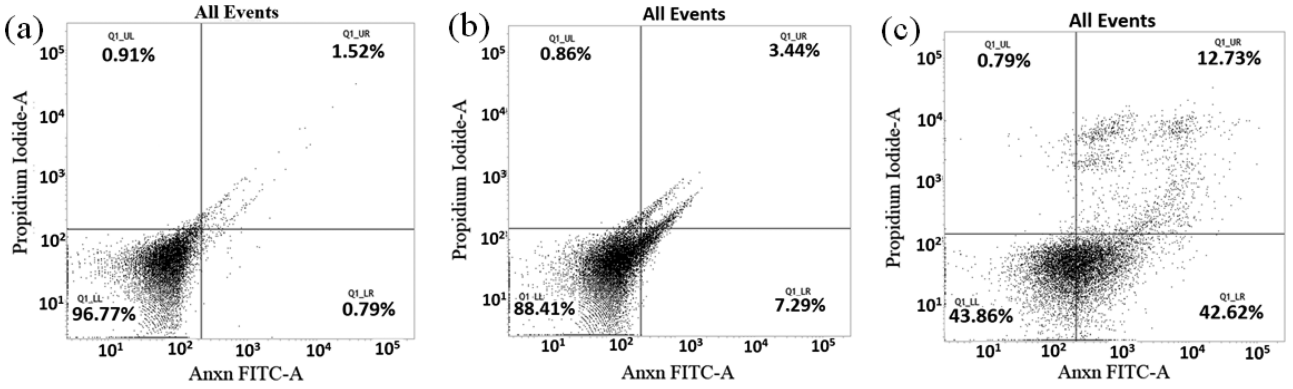

Figure 5. Annexin-V-FITC/PI-coupled flow cytometry analysis showing complex **6** (4 μM)-induced apoptosis in HeLa cells in the presence of visible light (400−700 nm, 10 J cm^{-2}): (a) only cells; (b) complex **6** + cell in the dark; (c) complex **6** + cell irradiated with visible light.

S66). The UV−visible spectrum of ABDA treated with complex **6** and irradiated with visible light (400−700 nm) revealed no notable changes, thereby ruling out the involvement of $^1O_2$ (type 2 pathway) in the observed phototoxicity of the complex. In another experiment, when complex **6** was treated with DCFDA and irradiated with visible light, the fluorescence intensity of DCF (an oxidation product of DCFDA) at 530 nm (λ_{ex} = 490 nm) decreased significantly in the presence of SOD and tiron (both are well-known superoxide radical scavengers), thereby suggesting the formation of superoxide anion radicals (Figure 6). However,

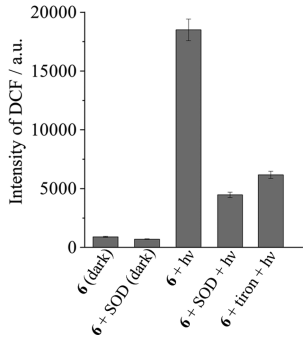

Figure 6. Fluorescence intensity of complex **6** (10 μM) treated with DCFDA at 530 nm (λ_{ex} = 490 nm) under various experimental conditions, suggesting the initial formation of the superoxide anion radical upon visible-light irradiation via a photoredox type 1 pathway and the subsequent formation of H_2O_2 by SOD (4 units) or tiron (0.5 mM).

in the presence of catalase (a well-known peroxide anion decomposer), the intensity of DCF remained unchanged. Interestingly, the emission intensity of DCF dropped markedly in the presence of both SOD and catalase as a result of diminishing concentrations of both superoxides and peroxides.[27] Thus, it follows that peroxide anions are the subsequent dismutation product of the superoxide anion radicals in the presence of SOD. To gain further evidence, we conducted a qualitative peroxide stick test.[4] When complex **6** was treated with SOD or tiron and irradiated with visible light, peroxide was detected, as evidenced by the appearance of a blue color on the stick (Figure S67). This observation again suggests that peroxides are formed from superoxide radical anions by a dismutation reaction. Under similar experimental conditions, the intensity of the blue color decreased significantly in the presence of both SOD and catalase owing to the simultaneous dismutation of superoxide radicals and decomposition of peroxide anions.[43] These observations suggest the involvement of superoxide radical species as ROS generated via a photoredox type 1 pathway.

DNA Binding. Given the mitochondrial localization of complex **6**, we envisioned that the mitochondrial DNA could be a target of the complex. Planar phenanthroline bases such as phen, dpq, and dppz are well-known to interact noncovalently with DNA via intercalation and groove binding.[57] Thus, we quantitatively studied the interaction of complexes **1**−**6** with ct-DNA by absorption spectral titrations, thermal denaturation, and viscosity measurements (Figure 7, Table 1, and Figure S68). Binding of a complex to DNA usually results in a gradual decrease in the intensity of the absorption band of a complex (hypochromism), from which the equilibrium binding constant (K_b) can be determined from the McGhee−von Hippel (MvH) equation (Figure 7a,b).[58] Complexes were found to interact significantly with ct-DNA, giving K_b values in the range of 10^4−10^5 M^{-1}. These values are suggestive of a noncovalent interaction of the complex with DNA. The dppz complexes **3** and **6** were found to bind with the strongest affinity, followed by the dpq (**2** and **5**) and phen (**1** and **4**) complexes. The binding propensity of the complexes is in accordance with the order of the planarity of the phenanthroline bases (dppz > dpq > phen). The parameter s in the MvH equation signifies the approximate number of DNA bases involved in interaction with the complex (s < 1.0 usually suggests molecular aggregation on the DNA surface).[30] The larger value of s for the dppz complexes also signifies their higher DNA binding affinity compared to those of the phen and dpq complexes.[30,58]

Next, we carried out a DNA melting study to obtain further insight into the DNA binding properties of complexes **1**−**6** (Figure 7c, Table 1, and Figure S69). Interaction of a drug with DNA typically results in an increase of the melting temperature of DNA (ΔT_m) as a result of stabilization of the double helix upon addition of the complex. A significant increase in the DNA melting temperature was observed in the presence of complex. The dppz complexes **3** and **6** resulted in the largest increase ($\Delta T_m \sim 5.5$), followed by the dpq ($\Delta T_m \sim 3.5$) and phen ($\Delta T_m \sim 1.8$) complexes. This observation suggests an increase in the stability of the double helix in the presence of complex, with the dppz complexes conferring the greatest stabilization, followed by the dpq and phen complexes. This trend in ΔT_m is again in accordance with the order of planarity of the phenanthroline bases (dppz > dpq > phen). The ΔT_m values suggest either groove binding (phen

https://doi.org/10.1021/acs.inorgchem.1c00444
Inorg. Chem. 2021, 60, 6649−6662

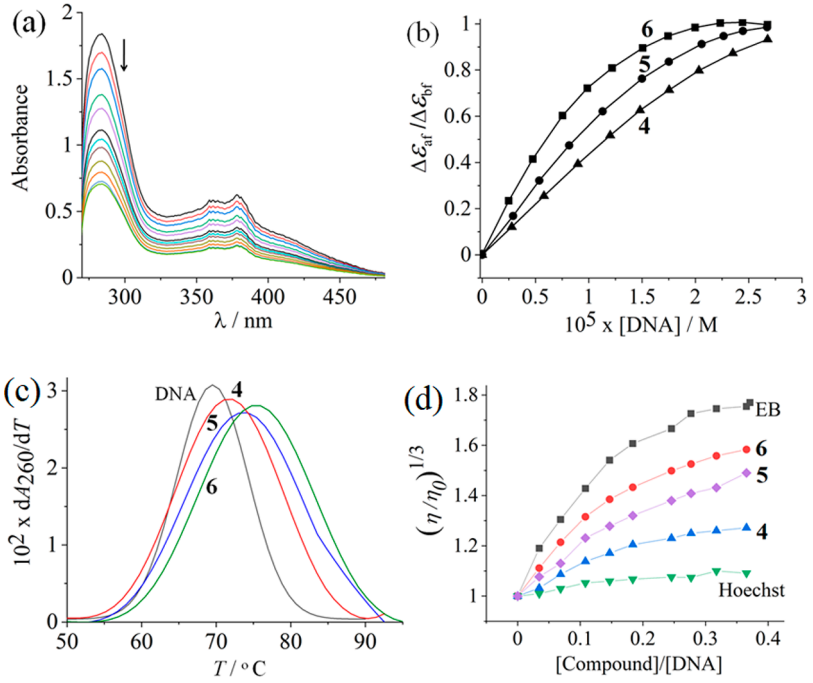

Figure 7. (a) Absorption spectral decrease of complex **6** in 5 mM Tris-HCl buffer (pH 7.2) upon an increase in the concentration of ct-DNA. (b) Least-squares nonlinear fit of $\Delta\varepsilon_{af}/\Delta\varepsilon_{bf}$ versus [DNA] for complexes **4** (▲), **5** (●), and **6** (■) to determine the binding constant (K_b) using the MvH equation. (c) Melting plots of ct-DNA (180 μM) alone (black) and in the presence of complexes **4** (red), **5** (blue), and **6** (olive). (d) Variation of the relative viscosity of ct-DNA (150 μM) at 37.0 (±0.1) °C in 5 mM Tris-HCl buffer (pH 7.2) containing 2.0–20% DMF as a function of the concentration of complex **4** (blue ▲), **2** (purple ◆), complex **3** (red ●), EB (black ■), and Hoechst 33258 (green ▼).

complexes) or partial intercalative binding (dpq and dppz complexes) of the complexes to ct-DNA.[59] Viscosity measurements were performed to study the effect of the added complex on the solution viscosity of ct-DNA (Figures 7d and S70). The relative specific viscosity η/η_0 (η and η_0 are the specific viscosities of a DNA solution in the presence and absence of the complex, respectively) of DNA is a qualitative measure of the increase in the contour length of DNA caused by the separation of base pairs. The well-known intercalator EB causes a considerable increase in the viscosity of DNA. In contrast, a partial and/or nonintercalative DNA binder could result in a small effect on the solution viscosity.[60a] The well-known DNA groove binder Hoechst 33258 was used as a reference compound showing an insignificant change of the viscosity. The viscosity changes observed for the complexes are suggestive of a two-step binding process in which the complex first interacts with the DNA surface followed by groove binding.[60b]

DNA Photocleavage. With the knowledge that complexes **1**–**6** bind to DNA with significant affinity, we were interested in accessing their ability to cleave DNA upon light irradiation. The photodamage of DNA by a photosensitizer disrupts vital cellular processes, thereby triggering the apoptotic pathway of cell death.[61] The cleavage of DNA induced by complexes **1**–**6** was studied using SC-pUC19-DNA by irradiating the samples with visible light of 446 nm and quantifying the amount of NC DNA formed (Figures 8 and S71). Complex **1** having photoinactive phen and cat^{2-} ligands did not show any notable DNA cleavage activity (8% NC). Complex **2** with dpq and cat^{2-} ligands showed moderate cleavage (52% NC) of DNA under similar conditions (lane 4 in Figure 8a). Complex **3** with the photoactive dppz ligand induced significant cleavage (81% NC) of SC-DNA upon light irradiation (lane 3 in Figure 8b).

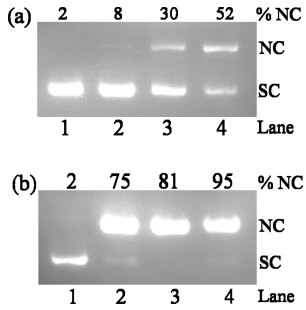

Figure 8. Cleavage of SC-pUC19-DNA (0.2 μg, 33.3 μM) by complexes **1**–**6** (10 μM) in 50 mM Tris-HCl/NaCl buffer (pH, 7.2) upon photoirradiation at 446 nm (50 mW) for 1 h: (a) lane 1, DNA control; lane 2, DNA + complex **1**; lane 3, DNA + complex **4**; lane 4, DNA + complex **2**; (b) lane 1, DNA control; lane 2, DNA + complex **5**, lane 3, DNA + complex **3**; lane 4, DNA + complex **6**.

For complexes **4**–**6**, the additional photosensitizing effect of the esc^{2-} ligand on the photocleavage activity was clearly evident. Complexes **4**–**6** showed significantly higher DNA photocleavage activity (30% NC for **4**, 75% NC for **5**, and 95% NC for **6**; lane 3 in Figure 8a and lanes 2 and 4 in Figure 8b, respectively) compared to their corresponding cat^{2-} analogues under similar conditions of light irradiation, suggesting the role of the photoactive esc^{2-} ligand in the overall DNA photocleavage activity. The DNA photocleavage activity follows the order **3** > **2** > **1** and **6** > **5** > **4**, which is in accordance with the order of the photosensitizing ability of the phenanthroline bases (dppz > dpq > phen). The complexes were not cleavage-active in the dark, thereby eliminating the possibility of hydrolytic DNA damage (Figure S72). The esculetin ligand alone showed ~40% photocleavage of DNA under similar conditions. Thus, a considerable increase of the DNA

https://doi.org/10.1021/acs.inorgchem.1c00444
Inorg. Chem. 2021, 60, 6649–6662

photocleavage activity of the esculetin ligand was observed upon coordination to cobalt(III).

Mechanistic Aspects of DNA Photocleavage. To identify the photocleavage pathway (type 1 or 2) and the actual DNA damaging species involved, we performed a photocleavage study using complex **6** in the presence of various radical scavengers and $^1O_2$ quenchers (Figures 9 and S73).[62]

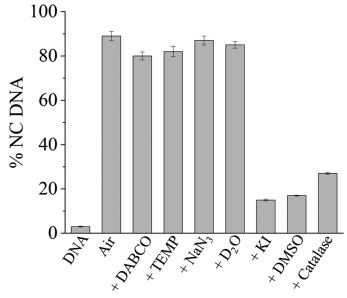

Figure 9. Bar diagram showing the photocleavage of SC-pUC19-DNA (0.2 μg, 33.3 μM) induced by complex **6** (10 μM) in the presence of various additives in Tris-HCl buffer (50 mM, pH 7.2). The additive concentrations/quantities are as follows: sodium azide, 0.5 mM; KI, 0.5 mM; TEMP, 0.5 mM; DABCO, 0.5 mM; D_2O, 16 μL; DMSO, 4 μL; catalase, 4 units; SOD, 4 units. Light source: visible light of 446 nm (50 mW). Irradiation time: 1 h.

The DNA photocleavage activity of complex **6** did not decrease noticeably in the presence of well-known $^1O_2$ quenchers such as 1,4-diazabicyclo[2.2.2]octane (DABCO), 2,2,6,6-tetramethyl-4-piperidone (TEMP), or sodium azide. Furthermore, no significant enhancement of the photocleavage activity of complex **6** was observed when the experiment was conducted in D_2O (a known enhancer of the $^1O_2$ lifetime) instead of H_2O.[63] These observations suggest that $^1O_2$ (type 2 pathway) is not involved in the DNA photocleavage activity of the complex. In contrast, the photocleavage activity of complex **6** was markedly inhibited in the presence of well-known hydroxyl radical ($HO^\bullet$) scavengers such as KI, DMSO, or catalase, thereby suggesting the involvement of $HO^\bullet$ (type 1 pathway) as the cleavage-active ROS. In a type 1 photoredox pathway, the cobalt(III) complex could undergo photoreduction to give a transient cobalt(II) species due to the transfer of an electron from the photoexcited dppz ligand to the cobalt(III) center. Subsequent interaction of the resulting cobalt(II) center with molecular oxygen reduces the latter to a superoxide anion, which eventually generates $HO^\bullet$ by the reaction $3O_2^{\bullet-} + 2H^+ \rightarrow HO^\bullet + HO^- + 2O_2$ (Figure S74). Such pathways are well documented in the literature for oxovandium(IV), iron(III), copper(II), and lanthanide(III) complexes with similar ligands.[22,27,64,65]

4. CONCLUSIONS

In summary, we have developed a series of novel mixed-ligand cobalt(III) complexes of the naturally occurring coumarin (esculetin) and phenanthroline bases (phen, dpq, and dppz) as dual-purpose photochemotherapeutic anticancer agents with remarkable phototoxic and cellular imaging properties. The esculetin complexes **4**–**6** showed significant toxicity in the presence of low-energy visible light but negligible toxicity in the absence of light against all cancer cell lines. Specifically, the dppz complex **6** bearing the photoactive esc^{2-} ligand showed the greatest activity, followed by the corresponding dpq (**5**) and phen (**4**) complexes. The corresponding complexes having the cat^{2-} ligand were considerably less phototoxic under similar conditions. The photocytotoxic activities of **1**–**6** correlated well with their lipophilicities (dppz > dpq > phen). Complex **6** accumulated within the mitochondria of HeLa cells, as revealed by a confocal microscopy study, and induced apoptotic cell death by generating ROS via a type 1 photoredox pathway. A significant reduction in the dark toxicity of the free esculetin ligand and the dppz base was observed upon coordination to cobalt(III). Complexes interacted with ct-DNA with significant affinity and photocleaved SC-DNA when irradiated with visible light via a type 1 photoredox mechanism involving a hydroxyl radical ($HO^\bullet$). In particular, complex **6** showing potent in vitro phototoxicity, a cellular imaging property, remarkable DNA binding, and DNA photocleavage activity is a potential new candidate as a next-generation photochemotherapeutic drug.

■ ASSOCIATED CONTENT

Supporting Information

The Supporting Information is available free of charge at https://pubs.acs.org/doi/10.1021/acs.inorgchem.1c00444.

Additional experimental details, reaction schemes (Figures S1 and S2), FT-IR spectra (Figures S3–S8), NMR spectra (Figures S9–S20), ESI-MS spectra (Figures S21–S26), UV–visible spectra (Figures S27 and S28), emission spectra (Figures S29 and S30), cyclic and square-wave voltammograms (Figures S31–S45), unit cell packing diagrams (Figures S46 and S47), DFT structures (Figures S48 and S49), stability studies (Figures S50–S53), MTT assay plots (Figures S54–S65), ROS generation (Figures S66 and S67), DNA binding plots (Figures S68–S70), DNA photocleavage (Figures S71–S74), crystallographic data (Table S1), Cartesian coordinates used for DFT calculations (Tables S2–S7), and solubility of complexes (Table S8) (PDF)

Accession Codes

CCDC 2024548 and 2024774 contain the supplementary crystallographic data for this paper. These data can be obtained free of charge via www.ccdc.cam.ac.uk/data_request/cif, or by emailing data_request@ccdc.cam.ac.uk, or by contacting The Cambridge Crystallographic Data Centre, 12 Union Road, Cambridge CB2 1EZ, UK; fax: +44 1223 336033.

■ AUTHOR INFORMATION

Corresponding Authors

Arun Kumar − *Department of Inorganic and Physical Chemistry, Indian Institute of Science, Bangalore 560012, Karnataka, India*; Email: kumar.arun.inor@gmail.com

Akhtar Hussain − *Department of Chemistry, Handique Girls' College, Guwahati 781001, Assam, India*; orcid.org/0000-0001-6742-3321; Email: akhtariisc@gmail.com

Authors

Tukki Sarkar − *Department of Chemistry, Handique Girls' College, Guwahati 781001, Assam, India*

Somarupa Sahoo − *Department of Inorganic and Physical Chemistry, Indian Institute of Science, Bangalore 560012, Karnataka, India*

Complete contact information is available at: https://pubs.acs.org/10.1021/acs.inorgchem.1c00444

https://doi.org/10.1021/acs.inorgchem.1c00444
Inorg. Chem. 2021, 60, 6649–6662

Notes

The authors declare no competing financial interest.

■ ACKNOWLEDGMENTS

A.H. thanks the Department of Biotechnology, Ministry of Science and Technology, Government of India, for financial assistance (Grants BT/PR25668/NER/95/1278/2017 and BT/401/NE/U-Excel/2013). T.S. thanks the Council for Scientific and Industrial Research (CSIR), New Delhi, India, for a Senior Research Fellowship (SRF) under the CSIR-Direct SRF scheme. We acknowledge the single-crystal X-ray diffraction facility of Gauhati University. We thank Dr. Kalyan Raidongia (Department of Chemistry, Indian Institute of Technology, Guwahati, India) for his generous help in obtaining the NMR spectra.

■ REFERENCES

(1) (a) Farrer, N. J.; Salassa, L.; Sadler, P. J. Photoactivated Chemotherapy (PACT): The Potential of Excited-State d-Block Metals in Medicine. *Dalton Trans.* **2009**, 10690−10701. (b) McKenzie, L. K.; Bryant, H. E.; Weinstein, J. A. Transition Metal Complexes as Photosensitisers in One- and Two-Photon Photodynamic Therapy. *Coord. Chem. Rev.* **2019**, *379*, 2−29.

(2) (a) Karges, J.; Heinemann, F.; Jakubaszek, M.; Maschietto, F.; Subecz, C.; Dotou, M.; Vinck, R.; Blacque, O.; Tharaud, M.; Goud, B.; Viñuelas Zahínos, E.; Spingler, B.; Ciofini, I.; Gasser, G. Rationally Designed Long-Wavelength Absorbing Ru(II) Polypyridyl Complexes as Photosensitizers for Photodynamic Therapy. *J. Am. Chem. Soc.* **2020**, *142*, 6578−6587. (b) Karges, J.; Yempala, T.; Tharaud, M.; Gibson, D.; Gasser, G. A Multiaction and Multitarget Ru(II)-Pt(IV) Conjugate Combining Cancer Activated Chemotherapy and Photodynamic Therapy to Overcome Drug Resistant Cancers. *Angew. Chem., Int. Ed.* **2020**, *59*, 7069−7075.

(3) Banerjee, S.; Chakravarty, A. R. Metal Complexes of Curcumin for Cellular Imaging, Targeting, and Photoinduced Anticancer Activity. *Acc. Chem. Res.* **2015**, *48*, 2075−2083.

(4) (a) Lo, K. K.-W. Luminescent Rhenium(I) and Iridium(III) Polypyridine Complexes as Biological Probes, Imaging Reagents, and Photocytotoxic Agents. *Acc. Chem. Res.* **2015**, *48*, 2985−2995. (b) Huang, H.; Banerjee, S.; Qiu, K.; Zhang, P.; Blacque, O.; Malcomson, T.; Paterson, M. J.; Clarkson, G. J.; Staniforth, M.; Stavros, V. G.; Gasser, G.; Chao, H.; Sadler, P. J. Targeted Photoredox Catalysis in Cancer Cells. *Nat. Chem.* **2019**, *11*, 1041−1048.

(5) Bonnett, R. *Chemical Aspects of Photodynamic Therapy*; Gordon and Breach Science Publishers: Singapore, 2000.

(6) (a) Celli, J. P.; Spring, B. Q.; Rizvi, I.; Evans, C. L.; Samkoe, K. S.; Verma, S.; Pogue, B. W.; Hasan, T. Imaging and Photodynamic Therapy: Mechanisms, Monitoring and Optimization. *Chem. Rev.* **2010**, *110*, 2795−2838. (b) Farrer, N. J.; Sadler, P. J. Photochemotherapy: Targeted Activation of Metal Anticancer Complexes. *Aust. J. Chem.* **2008**, *61*, 669−674.

(7) (a) Bonnett, R. Metal Complexes for Photodynamic Therapy. In *Comprehensive Coordination Chemistry*; McCleverty, J. A., Meyer, T., Eds.; Elsevier Pergamon, Oxford, U.K., 2004; Vol. 2, p 945. (b) Monro, S.; Colon, K. L.; Yin, H.; Roque, J., III; Konda, P.; Gujar, S.; Thummel, R. P.; Lilge, L.; Cameron, C. G.; McFarland, S. A. Transition Metal Complexes and Photodynamic Therapy from a Tumor-Centered Approach: Challenges, Opportunities, and Highlights from the Development of TLD1433. *Chem. Rev.* **2019**, *119*, 797−828. (c) McFarland, S. A.; Mandel, A.; Dumoulin-White, R.; Gasser, G. Metal-based Photosensitizers for Photodynamic Therapy: the Future of Multimodal Oncology? *Curr. Opin. Chem. Biol.* **2020**, *56*, 23−27.

(8) (a) Imberti, C.; Zhang, P.; Huang, H.; Sadler, P. J. New Designs for Phototherapeutic Transition Metal Complexes. *Angew. Chem., Int. Ed.* **2020**, *59*, 61−73. (b) Heinemann, F.; Karges, J.; Gasser, G. Critical Overview of the Use of Ru(II) Polypyridyl Complexes as Photosensitizers in One-Photon and Two-Photon Photodynamic Therapy. *Acc. Chem. Res.* **2017**, *50*, 2727−2736.

(9) (a) Coogan, M. P.; Fernández-Moreira, V. Progress with, and Prospects for, Metal Complexes in Cell Imaging. *Chem. Commun.* **2014**, *50*, 384−399. (b) Fernández-Moreira, V.; Thorp-Greenwood, F. L.; Coogan, M. P. Application of d^6 Transition Metal Complexes in Fluorescence Cell Imaging. *Chem. Commun.* **2010**, *46*, 186−202.

(10) Pöthig, A.; Casini, A. Recent Developments of Supramolecular Metal-based Structures for Applications in Cancer Therapy and Imaging. *Theranostics* **2019**, *9*, 3150−3169.

(11) (a) Roy, S.; Saha, S.; Majumdar, R.; Dighe, R. R.; Chakravarty, A. R. Photocytotoxic 3d-Metal Scorpionates with a 1,8-Naphthalimide Chromophore Showing Photoinduced DNA and Protein Cleavage Activity. *Inorg. Chem.* **2009**, *48*, 9501−9509. (b) Basu, U.; Khan, I.; Hussain, A.; Kondaiah, P.; Chakravarty, A. R. Photodynamic Effect in Near-IR Light by a Photocytotoxic Iron(III) Cellular Imaging Agent. *Angew. Chem.* **2012**, *124*, 2712−2715.

(12) Deka, B.; Sarkar, T.; Banerjee, S.; Kumar, A.; Mukherjee, S.; Deka, S.; Saikia, K. K.; Hussain, A. Novel Mitochondria Targeted Copper(II) Complexes of Ferrocenyl Terpyridine and Anticancer Active 8-Hydroxyquinolines Showing Remarkable Cytotoxicity, DNA and Protein Binding Affinity. *Dalton Trans.* **2017**, *46*, 396−409.

(13) (a) Banik, B.; Somyajit, K.; Nagaraju, G.; Chakravarty, A. R. Oxovanadium(IV) catecholates of terpyridine bases for cellular imaging and photocytotoxicity in red light. *RSC Adv.* **2014**, *4*, 40120−40131. (b) Bhattacharyya, U.; Kumar, B.; Garai, A.; Bhattacharyya, A.; Kumar, A.; Banerjee, S.; Kondaiah, P.; Chakravarty, A. R. Curcumin "Drug" Stabilized in Oxidovanadium-(IV)-BODIPY Conjugates for Mitochondria-Targeted Photocytotoxicity. *Inorg. Chem.* **2017**, *56*, 12457−12468.

(14) Mukherjee, N.; Raghavan, A.; Podder, S.; Majumdar, S.; Kumar, A.; Nandi, D.; Chakravarty, A. R. Photocytotoxic Activity of Copper (II) and Zinc (II) Complexes of Curcumin and (Acridinyl) dipyridophenazine. *ChemistrySelect* **2019**, *4*, 9647−9658.

(15) Pradeepa, M.; Bhojya Naik, H. S.; Vinay Kumar, B.; Indira Priyadarsini, K.; Barik, A.; Jayakumar, S. Synthesis and Characterization of Cobalt(II), Nickel(II) and Copper(II)-based Potential Photosensitizers: Evaluation of their DNA Binding Profile, Cleavage and Photocytotoxicity. *Inorg. Chim. Acta* **2015**, *428*, 138−146.

(16) Karges, J.; Basu, U.; Blacque, O.; Chao, H.; Gasser, G. Polymeric Encapsulation of Novel Homoleptic Bis(dipyrrinato) Zinc(II) Complexes with Long Lifetimes for Applications as Photodynamic Therapy Photosensitisers. *Angew. Chem., Int. Ed.* **2019**, *58*, 14334−14340.

(17) (a) Lahiri, D.; Roy, S.; Saha, S.; Majumdar, R.; Dighe, R. R.; Chakravarty, A. R. Anaerobic DNA Cleavage Activity in Red Light and Photocytotoxicity of (pyridine-2-thiol)Cobalt(III) Complexes of Phenanthroline Bases. *Dalton Trans.* **2010**, *39*, 1807−1816. (b) Roy, S.; Roy, S.; Saha, S.; Majumdar, R.; Dighe, R. R.; Jemmis, E. D.; Chakravarty, A. R. Cobalt(II) Complexes of Terpyridine Bases as Photochemotherapeutic Agents Showing Cellular Uptake and Photocytotoxicity in Visible Light. *Dalton Trans.* **2011**, *40*, 1233−1242. (c) Saha, S.; Majumdar, R.; Dighe, R. R.; Chakravarty, A. R. Enhanced Photodynamic Effect of Cobalt(III) Dipyridophenazine Complex on Thyrotropin Receptor Expressing HEK293 Cells. *Metallomics* **2010**, *2*, 754−765.

(18) Arounaguiri, S.; Maiya, B. G. Dipyridophenazine Complexes of Cobalt(III) and Nickel(II): DNA-Binding and Photocleavage Studies. *Inorg. Chem.* **1996**, *35*, 4267−4270.

(19) Munteanu, C. R.; Suntharalingam, K. Advances in Cobalt Complexes as Anticancer Agents. *Dalton Trans.* **2015**, *44*, 13796−13808.

(20) (a) Renfrew, A. K.; Bryce, N. S.; Hambley, T. W. Delivery and Release of Curcumin by a Hypoxia-Activated Cobalt Chaperone: a XANES and FLIM Study. *Chem. Sci.* **2013**, *4*, 3731−3739. (b) Kim, B. J.; Hambley, T. W.; Bryce, N. S. Visualising the Hypoxia Selectivity of Cobalt(III) Prodrugs. *Chem. Sci.* **2011**, *2*, 2135−2142. (c) Batista, C. R.; da Silva Miranda, F.; Pinheiro, C. B.; Lanznaster, M. An

https://doi.org/10.1021/acs.inorgchem.1c00444
Inorg. Chem. 2021, 60, 6649−6662

Esculetin−Cobalt(III) Archetype for Redox-Activated Drug Delivery Platforms with Hypoxic Selectivity. *Eur. J. Inorg. Chem.* **2018**, *2018*, 612−616.
(21) (a) Renfrew, A. K.; Bryce, N. S.; Hambley, T. Cobalt(III) Chaperone Complexes of Curcumin: Photoreduction, Cellular Accumulation and Light-Selective Toxicity towards Tumour Cells. *Chem. - Eur. J.* **2015**, *21*, 15224−15234. (b) Garai, A.; Pant, I.; Banerjee, S.; Banik, B.; Kondaiah, P.; Chakravarty, A. R. Photorelease and Cellular Delivery of Mitocurcumin from its Cytotoxic Cobalt(III) Complex in Visible Light. *Inorg. Chem.* **2016**, *55*, 6027−6035.
(22) Sarkar, T.; Banerjee, S.; Hussain, A. Remarkable Visible Light-Triggered Cytotoxicity of Mitochondria Targeting Mixed-Ligand Cobalt(III) Complexes of Curcumin and Phenanthroline Bases Binding to Human Serum Albumin. *RSC Adv.* **2015**, *5*, 16641−16653.
(23) Ma, D.-L.; Wu, C.; Cheng, S.-S.; Lee, F.-W.; Han, Q.-B.; Leung, C.-H. Development of Natural Product-Conjugated Metal Complexes as Cancer Therapies. *Int. J. Mol. Sci.* **2019**, *20*, 341.
(24) (a) Mansoori, A.; Mohammadi, A.; Amin Doustvandi, M.; Mohammadnejad, F.; Kamari, F.; Gjerstorff, M. F.; Baradaran, B.; Hamblin, M. R. Photodynamic Therapy for Cancer: Role of Natural Products. *Photodiagn. Photodyn. Ther.* **2019**, *26*, 395−404. (b) Xiao, Q.; Wu, J.; Pang, X.; Jiang, Y.; Wang, P.; Leung, A. W.; Gao, L.; Jiang, S.; Xu, C. Discovery and Development of Natural Products and their Derivatives as Photosensitizers for Photodynamic Therapy. *Curr. Med. Chem.* **2018**, *25*, 839−860.
(25) Zamojc, K.; Zdrowowicz, M.; Wiczk, W.; Jacewicz, D.; Chmurzynski, L. Dihydroxycoumarins as Highly Selective Fluorescent Probes for the Fast Detection of 4-Hydroxy-TEMPO in Aqueous Solution. *RSC Adv.* **2015**, *5*, 63807−63812.
(26) (a) Hausen, M.; Schmieder, M. The Sensitizing Capacity of Coumarins (I). *Contact Dermatitis* **1986**, *15*, 157−163. (b) Zhang, L.; Dong, S.; Zhu, L. Fluorescent Dyes of the Esculetin and Alizarin Families Respond to Zinc Ions Ratiometrically. *Chem. Commun.* **2007**, 1891−1893.
(27) Sarkar, T.; Bhattacharyya, A.; Banerjee, S.; Hussain, A. LMCT Transition-based Red-Light Photochemotherapy Using a Tumour-Selective Ferrocenyl Iron(III) Coumarin Conjugate. *Chem. Commun.* **2020**, *56*, 7981−7984.
(28) (a) Marrache, S.; Pathak, R. K.; Dhar, S. Detouring of Cisplatin to Access Mitochondrial Genome for Overcoming Resistance. *Proc. Natl. Acad. Sci. U. S. A.* **2014**, *111*, 10444−10449. (b) Sarkar, T.; Banerjee, S.; Mukherjee, S.; Hussain, A. Mitochondrial Selectivity and Remarkable Photocytotoxicity of a Ferrocenyl Neodymium(III) Complex of Terpyridine and Curcumin in Cancer Cells. *Dalton Trans.* **2016**, *45*, 6424−6438.
(29) (a) Fulda, S.; Galluzzi, L.; Kroemer, G. Targeting Mitochondria for Cancer Therapy. *Nat. Rev. Drug Discovery* **2010**, *9*, 447−464. (b) Basu, A.; Krishnamurthy, S. Cellular Responses to Cisplatin-Induced DNA Damage. *J. Nucleic Acids* **2010**, *2010*, 201367.
(30) (a) Angeles-Boza, A. M.; Bradley, P. M.; Fu, P. K.-L.; Wicke, S. E.; Bacsa, J.; Dunbar, K. R.; Turro, C. DNA Binding and Photocleavage in Vitro by New Dirhodium(II) dppz Complexes: Correlation to Cytotoxicity and Photocytotoxicity. *Inorg. Chem.* **2004**, *43*, 8510−8519. (b) Gill, M. R.; Thomas, J. A. Ruthenium(II) Polypyridyl Complexes and DNA-from Structural Probes to Cellular Imaging and Therapeutics. *Chem. Soc. Rev.* **2012**, *41*, 3179−3192.
(31) Perrin, D. D.; Armarego, W. L. F.; Perrin, D. R. *Purification of Laboratory Chemicals*; Pergamon Press: Oxford, U.K., 1980.
(32) (a) Dickeson, J. E.; Summers, L. A. Derivatives of 1,10-Phenanthroline-5,6-Quinone. *Aust. J. Chem.* **1970**, *23*, 1023−1027. (b) Collins, J. G.; Sleeman, A. D.; Aldrich-Wright, J. R.; Greguric, I.; Hambley, T. W. A ^{1}H NMR Study of the DNA Binding of Ruthenium(II) Polypyridyl Complexes. *Inorg. Chem.* **1998**, *37*, 3133−3141.
(33) Amouyal, E.; Homsi, A.; Chambron, J.-C.; Sauvage, J.-P. Synthesis and Study of a Mixed-Ligand Ruthenium(II) Complex in its Ground and Excited States: Bis(2,2′-bipyridine)(dipyrido[3,2-a:2′,3′-c]phenazine-N^4N^5)ruthenium(II). *J. Chem. Soc., Dalton Trans.* **1990**, 1841−1845.
(34) Vlcek, A. A. Preparation of Co(dipy)2 × 2+ Complexes (X- = Chloride, Bromide, Iodide, Nitrite) by Controlled Oxidative Processes. *Inorg. Chem.* **1967**, *6*, 1425−1427.
(35) Jones, G., II; Jackson, J. R.; Choi, C.; Bergmark, W. R. Solvent Effects on Emission Yield and Lifetime for Coumarin Laser Dyes. Requirements for a Rotatory Decay Mechanism. *J. Phys. Chem.* **1985**, *89*, 294−300.
(36) (a) Lakowicz, J. R. *Principles of Fluorescence Spectroscopy*; Kluwer Academic/Plenum Publishers: New York, 1999. (b) Williams, A. T. R.; Winfield, S. A.; Miller, J. N. Relative Fluorescence Quantum Yields Using a Computer-Controlled Luminescence Spectrometer. *Analyst* **1983**, *108*, 1067−1071.
(37) Sheldrick, G. M. *SHELX-2013, Programs for Crystal Structure Solution and Refinement*; University of Göttingen: Göttingen, Germany, 2013.
(38) (a) Walker, N.; Stuart, D. An Empirical Method for Correcting Diffractometer Data for Absorption Effects. *Acta Crystallogr., Sect. A: Found. Crystallogr.* **1983**, *39*, 158−166. (b) Farrugia, L. J. WinGX Suite for Small-Molecule Single-Crystal Crystallography. *J. Appl. Crystallogr.* **1999**, *32*, 837−838. (c) Farrugia, L. J. *WinGX*, version 1.65.04; Department of Chemistry, University of Glasgow: Glasgow, Scotland, 2003.
(39) Johnson, C. K. *ORTEP-II: A FORTRAN Thermal-Ellipsoid Plot Program for Crystal Structure Illustrations*; Oak Ridge National Laboratory: Oak Ridge, TN, 1976; Report ORNL-5138.
(40) (a) Lee, C.; Yang, W.; Parr, R. G. Development of the Colle-Salvetti Correlation-Energy Formula into a Functional of the Electron Density. *Phys. Rev. B: Condens. Matter Mater. Phys.* **1988**, *37*, 785−789. (b) Frisch, M. J.; Trucks, G. W.; Schlegel, H. B.; Scuseria, G. E.; Robb, M. A.; Cheeseman, J. R.; Montgomery, J. A., Jr.; Vreven, T.; Kudin, K. N.; Burant, J. C.; Millam, J. M.; Iyengar, S. S.; Tomasi, J.; Barone, V.; Mennucci, B.; Cossi, M.; Scalmani, G.; Rega, N.; Petersson, G. A.; Nakatsuji, H.; Hada, M.; Ehara, M.; Toyota, K.; Fukuda, R.; Hasegawa, J.; Ishida, M.; Nakajima, T.; Honda, Y.; Kitao, O.; Nakai, H.; Klene, M.; Li, X.; Knox, J. E.; Hratchian, H. P.; Cross, J. B.; Bakken, V.; Adamo, C.; Jaramillo, J.; Gomperts, R.; Stratmann, R. E.; Yazyev, O.; Austin, A. J.; Cammi, R.; Pomelli, C.; Ochterski, J. W.; Ayala, P. Y.; Morokuma, K.; Voth, G. A.; Salvador, P.; Dannenberg, J. J.; Zakrzewski, V. G.; Dapprich, S.; Daniels, A. D.; Strain, M. C.; Farkas, O.; Malick, D. K.; Rabuck, A. D.; Raghavachari, K.; Foresman, J. B.; Ortiz, J. V.; Cui, Q.; Baboul, A. G.; Clifford, S.; Cioslowski, J.; Stefanov, B. B.; Liu, G.; Liashenko, A.; Piskorz, P.; Komaromi, I.; Martin, R. L.; Fox, D. J.; Keith, T.; Al-Laham, M. A.; Peng, C. Y.; Nanayakkara, A.; Challacombe, M.; Gill, P. M. W.; Johnson, B.; Chen, W.; Wong, M. W.; Gonzalez, C.; Pople, J. A. *Gaussian 03*, revision B.4; Gaussian Inc.: Pittsburgh, PA, 2003.
(41) Mosmann, T. Rapid Colorimetric Assay for Cellular Growth and Survival: Application to Proliferation and Cytotoxicity Assays. *J. Immunol. Methods* **1983**, *65*, 55−63.
(42) Soni, C.; Karande, A. A. Glycodelin A suppresses the Cytolytic Activity of CD8+ T Lymphocytes. *Mol. Immunol.* **2010**, *47*, 2458−2466.
(43) (a) Zheng, Z.; Zhang, T.; Liu, H.; Chen, Y.; Kwok, R. T. K.; Ma, C.; Zhang, P.; Sung, H. H. Y.; Williams, I. D.; Lam, J. W. Y.; Wong, K. S.; Tang, B. Z. Bright Near-Infrared Aggregation-Induced Emission Luminogens with Strong Two-Photon Absorption, Excellent Organelle Specificity, and Efficient Photodynamic Therapy Potential. *ACS Nano* **2018**, *12*, 8145−8159. (b) Novohradsky, V.; Vigueras, G.; Pracharova, J.; Cutillas, N.; Janiak, C.; Kostrhunova, H.; Brabec, V.; Ruiz, J.; Kasparkova, J. Molecular Superoxide Radical Photogeneration in Cancer Cells by Dipyridophenazine Iridium(III) Complexes. *Inorg. Chem. Front.* **2019**, *6*, 2500−2513.
(44) Yuan, Y.; Zhang, C.-J.; Liu, B. A Platinum Prodrug Conjugated with a Photosensitizer with Aggregation-Induced Emission (AIE) Characteristics for Drug Activation Monitoring and Combinatorial Photodynamic−Chemotherapy Against Cisplatin Resistant Cancer Cells. *Chem. Commun.* **2015**, *51*, 8626−8629.
(45) Martin, N. M.; Friedlander, A.; Mok, A.; Kent, D.; Wiedmann, M.; Boor, K. J. Peroxide Test Strips Detect Added Hydrogen Peroxide

https://doi.org/10.1021/acs.inorgchem.1c00444
Inorg. Chem. 2021, 60, 6649−6662

in Raw Milk at Levels Affecting Bacterial Load. *J. Food Prot.* **2014**, *77*, 1809−1813.
(46) Nakamoto, K. *Infrared and Raman Spectra of Inorganic and Coordination Compounds*, 3rd ed.; John Wiley & Sons: New York, 1978.
(47) Geary, W. J. The Use of Conductivity Measurements in Organic Solvents for the Characterisation of Coordination Compounds. *Coord. Chem. Rev.* **1971**, *7*, 81−122.
(48) Wicklund, P. A.; Brown, D. G. Synthesis and Characterization of Some Cobalt(III) Catechol Complexes. *Inorg. Chem.* **1976**, *15*, 396−400.
(49) Hussain, A.; Lahiri, D.; Ameerunisha Begum, M. S.; Saha, S.; Majumdar, R.; Dighe, R. R.; Chakravarty, A. R. Photocytotoxic Lanthanum(III) and Gadolinium(III) Complexes of Phenanthroline Bases Showing Light-Induced DNA Cleavage Activity. *Inorg. Chem.* **2010**, *49*, 4036−4045.
(50) Davies, C. J.; Solan, G. A.; Fawcett, J. Synthesis and Structural Characterisation of Cobalt(II) and Iron(II) Chloride Complexes Containing Bis(2-pyridylmethyl)amine and Tris(2-pyridylmethyl)-amine Ligands. *Polyhedron* **2004**, *23*, 3105−3114.
(51) Kitson, R. E. Simultaneous Spectrophotometric Determination of Cobalt, Copper, and Iron. *Anal. Chem.* **1950**, *22*, 664−667.
(52) Horter, D.; Dressman, J. B. Influence of Physicochemical Properties on Dissolution of Drugs in the Gastrointestinal Tract. *Adv. Drug Delivery Rev.* **2001**, *46*, 75−87.
(53) (a) Prasad, P.; Sasmal, P. K.; Khan, I.; Kondaiah, P.; Chakravarty, A. R. Schiff Base Oxovanadium(IV) Complexes of Phenanthroline Bases Showing DNA Photocleavage Activity at Near-IR Light and Photocytotoxicity. *Inorg. Chim. Acta* **2011**, *372*, 79−87. (b) Prasad, P.; Sasmal, P. K.; Majumdar, R.; Dighe, R. R.; Chakravarty, A. R. Photocytotoxicity and Near-IR Light DNA Cleavage Activity of Oxovanadium(IV) Schiff Base Complexes having Phenanthroline Bases. *Inorg. Chim. Acta* **2010**, *363*, 2743−2751.
(54) Delaey, E.; van Laar, F.; De Vos, D.; Kamuhabwa, A.; Jacobs, P.; de Witte, P. A Comparative Study of the Photosensitizing Characteristics of Some Cyanine Dyes. *J. Photochem. Photobiol., B* **2000**, *55*, 27−36.
(55) Leonidova, A.; Pierroz, V.; Rubbiani, R.; Heier, J.; Ferrari, S.; Gasser, G. Towards Cancer Cell-Specific Phototoxic Organometallic Rhenium(I) Complexes. *Dalton Trans.* **2014**, *43*, 4287−4294.
(56) Yuan, Y.; Zhang, C.-J.; Xu, S.; Liu, B. A Self-Reporting AIE Probe with a Built-in Singlet Oxygen Sensor for Targeted Photodynamic Ablation of Cancer Cells. *Chem. Sci.* **2016**, *7*, 1862−1866.
(57) (a) Liu, H.-K.; Sadler, P. J. Metal Complexes as DNA Intercalators. *Acc. Chem. Res.* **2011**, *44*, 349−359. (b) Barton, J. K.; Danishefsky, A.; Goldberg, J. Tris(phenanthroline)ruthenium(II): Stereoselectivity in Binding to DNA. *J. Am. Chem. Soc.* **1984**, *106*, 2172−2176.
(58) McGhee, J. D.; von Hippel, P. H. Theoretical Aspects of DNA-Protein Interactions: Co-operative and Non-co-operative Binding of Large Ligands to a One-Dimensional Homogeneous Lattice. *J. Mol. Biol.* **1974**, *86*, 469−489.
(59) (a) An, Y.; Liu, S.-D.; Deng, S.-Y.; Ji, L.-N.; Mao, Z.-W. Cleavage of Double-Strand DNA by Linear and Triangular Trinuclear Copper Complexes. *J. Inorg. Biochem.* **2006**, *100*, 1586−1593. (b) Eichhorn, G. L.; Shin, Y. A. Interaction of Metal Ions with Polynucleotides and Related Compounds. XII. The Relative Effect of Various Metal Ions on DNA Helicity. *J. Am. Chem. Soc.* **1968**, *90*, 7323−7328.
(60) (a) Veal, J. M.; Rill, R. L. Noncovalent DNA Binding of Bis(1,10-phenanthroline)copper(I) and Related Compounds. *Biochemistry* **1991**, *30*, 1132−1140. (b) Pellegrini, P. P.; Aldrich-Wright, J. R. Evidence for Chiral Discrimination of Ruthenium(II) Polypyridyl Complexes by DNA. *Dalton Trans.* **2003**, 176−183.
(61) Schatzschneider, U. Photoactivated Biological Activity of Transition-Metal Complexes. *Eur. J. Inorg. Chem.* **2010**, *2010*, 1451−1467.
(62) Szacilowski, K.; Macyk, W.; Drzewiecka-Matuszek, A.; Brindell, M.; Stochel, G. Bioinorganic Photochemistry: Frontiers and Mechanisms. *Chem. Rev.* **2005**, *105*, 2647−2694.
(63) (a) Khan, A. U. Singlet Molecular Oxygen. A New Kind of Oxygen. *J. Phys. Chem.* **1976**, *80*, 2219−2228. (b) Merkel, P. B.; Nilsson, R.; Kearns, D. R. Deuterium Effects on Singlet Oxygen Lifetimes in Solutions. New Test of Singlet Oxygen Reactions. *J. Am. Chem. Soc.* **1972**, *94*, 1030−1031.
(64) Banerjee, S.; Dixit, A.; Karande, A. A.; Chakravarty, A. R. Remarkable Selectivity and Photo-Cytotoxicity of an Oxidovanadium-(IV) Complex of Curcumin in Visible Light. *Eur. J. Inorg. Chem.* **2015**, *2015*, 447−457.
(65) Kunkely, H.; Vogler, A. Photoredox Reactivity of Iron(III) Phenolates in Aqueous Solution Induced by Ligand-to-Metal Charge Transfer Excitation. *Inorg. Chem. Commun.* **2003**, *6*, 1335−1337.

https://doi.org/10.1021/acs.inorgchem.1c00444
Inorg. Chem. 2021, 60, 6649−6662